Structure-Based Design of a Highly Immunogenic, Conformationally Stabilized FimH Antigen for a Urinary Tract Infection Vaccine

Authors: Natalie C. Silmon de Monerri PhD[1]*, Ye Che PhD[2+], Joshua A. Lees PhD[2], Jayasankar Jasti PhD[2+], Huixian Wu PhD[2], Matthew C. Griffor[2+], Srinivas Kodali[1], Julio Caesar Hawkins[1], Jacqueline Lypowy[1], Christopher Ponce[1], Kieran Curley[1], Alexandre Esadze PhD[1], Juan Carcamo PhD[1+], David Keeney[1+], Arthur Illenberger[1+], Yury V. Matsuka PhD[1+], Suman Shanker[2+], Laurent Chorro PhD[1+], Alexey V. Gribenko PhD[1], Seungil Han PhD[2], Annaliesa S. Anderson PhD FAAM[1], Robert G. K. Donald PhD[1]

Affiliations:

[1] Vaccine Research and Development, Pfizer Inc; Pearl River, NY 10965, USA.

[2] Discovery Sciences, Pfizer Inc.; Groton, CT 06340, USA.

[+]Former Pfizer employee

*Corresponding author email: natalie.silmondemonerri@pfizer.com

One sentence summary: Structure-based design of a conformationally stabilized *E. coli* FimH vaccine candidate capable of eliciting antibodies to diverse epitopes with the ability to block bacterial binding to bladder epithelial cells.

Abstract: Adhesion of *E. coli* to the urinary tract epithelium is a critical step in establishing urinary tract infections. FimH is an adhesin positioned on the fimbrial tip which binds to mannosylated proteins on the urinary tract epithelium via its lectin domain ($FimH_{LD}$). FimH is of interest as a target of vaccines to prevent urinary tract infections (UTI). Previously, difficulties in obtaining purified recombinant FimH from *E. coli* along with the poor inherent immunogenicity of FimH have hindered the development of effective FimH vaccine candidates. To overcome these challenges, we have devised a novel production method using mammalian cells to produce high yields of homogeneous FimH protein with comparable biochemical and immunogenic properties to FimH produced in *E. coli.* Next, to optimize conformational stability and immunogenicity of FimH, we used a computational approach to design improved FimH mutants and evaluated their biophysical and biochemical properties, and murine immunogenicity. This approach identified a highly immunogenic FimH variant (FimH-DSG TM) that is produced at high yields in mammalian cells. By x-ray crystallography, we confirmed that the stabilized structure of the $FimH_{LD}$ in FimH-DSG TM is similar to native FimH on the fimbrial tip. Characterization of monoclonal antibodies elicited by FimH-DSG TM that can block bacterial binding to mannosylated surfaces identified 4 non-overlapping binding sites whose epitopes were mapped via a combinatorial cryogenic electron microscopy approach. Novel inhibitory epitopes in the lectin binding FimH were identified, revealing diverse functional mechanisms of FimH-directed antibodies with relevance to FimH-targeted UTI vaccines.

Author summary:

Escherichia coli is the primary cause of urinary tract infections. Adherence to uroepithelial surfaces is mediated by the pilus adhesin protein FimH, which is of interest as a vaccine candidate. We developed a method for producing recombinant FimH at bioprocess scale, previously a barrier to commercial development. Structure-based design and screening was used to identify a novel FimH vaccine candidate with improved stability and immunogenicity in mice. Structure of this full-length protein was determined by X-ray crystallography and shown to closely resemble the pilus adhesin present in its native form on the bacterial surface. Binding sites of biologically active FimH monoclonal antibodies were determined by X-ray crystallography or by cryo-electron microscopy, providing insights into mechanisms by which antibodies block binding of the bacteria to urinary tract receptors.

Introduction:

Uncomplicated urinary tract infections (UTI) affect approximately 50% of women at least once during their lifetime (1). In addition, sepsis-associated in-hospital mortality is significantly linked to UTI, resulting in a substantial burden on healthcare systems. Multidrug-resistant bacteria are frequently associated with UTI, which impacts routine urological practices (2). While several organisms can cause UTI, the most common agent is uropathogenic *Escherichia coli* (UPEC), which is associated with 75% of uncomplicated and 65% of complicated UTI (3). UPEC colonize the gastrointestinal tract and migrate from the fecal flora to the urogenital tract, where they adhere to host uroepithelial cells and establish a reservoir for ascending infections of the urinary tract (4). Adhesion is facilitated by fimbrial adhesins located on the bacterial surface, including type 1 fimbriae, which bind to mannosylated glycoproteins on bladder epithelial cells (5) as well as those secreted into the urine e.g. uromodulin (6).

Type 1 fimbriae are highly conserved among clinical UPEC isolates and are encoded by the *fim* gene cluster, which encodes chaperone and usher proteins (FimC, FimD), various structural subunits (FimA, FimF, FimG), and an adhesin called FimH that is displayed on the fimbrial tip (7). FimH is essential for all characteristics of UTI in mouse models that mimic aspects of human UPEC bladder infection: it mediates adhesion to target cells, intracellular invasion, biofilm formation, and resistance to killing by neutrophils (8-10). FimH is under positive selection in *E. coli* human cystitis isolates and positively selected residues have been proposed to influence virulence in mouse models of cystitis (11). In addition, it is important for uroepithelial cell shedding and invasion of bladder cells by *E. coli* (12, 13). Small molecule inhibitors that target FimH by mimicking mannosylated receptors are efficacious against UTI in animal models, further validating the role of FimH in UTI (14, 15).

FimH is composed of two domains, an N-terminal lectin binding domain ($FimH_{LD}$) responsible for binding to the terminal mannose moiety on epithelial glycoproteins, and a C-terminal pilin domain ($FimH_{PD}$). $FimH_{PD}$ serves to link FimH to other structural subunits of the pilus such as FimG, through a mechanism called donor strand complementation (16). $FimH_{PD}$ possesses an incomplete immunoglobulin-like fold, containing a groove that provides a binding site for the donor N-terminal β-strand of FimG, which when bound forms a strong intermolecular linkage with FimH. While $FimH_{LD}$ can be expressed in a soluble, stable form, full-length FimH is unstable unless produced as a complex with the chaperone FimC or complemented with the FimG N-terminal donor strand peptide (as an exogenous peptide or directly fused to FimH via a polypeptide linker) (17, 18). $FimH_{LD}$ transitions between two endpoint conformations: a ‘closed’ conformation with a high affinity for mannosylated proteins, and an ‘open’ conformation with a relatively compressed structure, a wide mannose binding pocket, that binds to mannosylated

proteins with low affinity (19). Conformation and ligand-binding properties of $FimH_{LD}$ are under the allosteric control of $FimH_{PD}$, which itself exhibits only minor structural changes upon ligand binding (20, 21). Under static conditions, interaction between the lectin and pilin domains stabilizes $FimH_{LD}$ in a low-affinity, open conformation (21, 22). Upon binding to a mannose derivative (mannoside) ligand, $FimH_{LD}$ undergoes a conformational change leading to a high affinity state (with a 1000 to 100,000-fold higher affinity for mannose (21)), where the $FimH_{LD}$ and $FimH_{PD}$ remain in close contact. In the absence of negative allosteric regulation exerted by the $FimH_{PD}$, isolated recombinant $FimH_{LD}$ is locked in the high-affinity state and is highly stable (19).

FimH is a key target for development of candidate vaccines to prevent UTI. The proposed primary mechanism of action of a FimH vaccine is inhibition of bacterial adhesion to urinary tract epithelial cells (23). Immunization with recombinant $FimH_{LD}$ or full length FimH in complex with FimC (FimCH) is protective in both mouse and non-human primate models of UTI (23-32). Safety and immunogenicity of four doses of FimCH combined with a TLR4 adjuvant has been evaluated in humans in a Phase 1 study (33). In this exploratory analysis, female subjects with recurrent UTI had fewer UTI episodes following immunization, suggesting that the vaccine may reduce their frequency.

Development of FimH vaccines has been hindered significantly by two major issues: low yield of recombinant protein in *E. coli* and the requirement for multiple doses to elicit immune responses against *E. coli (33, 34)*. In native *E. coli,* FimH is produced in the periplasm which facilitates disulfide bond formation (35). Typical yields of recombinant FimH reported at lab-bench scale are 3-5 mg/L for the purified FimCH complex and 4-10 mg/L for $FimH_{LD}$ (18, 19); therefore, although the antigen has promise, it cannot be made in high enough quantities to proceed with clinical evaluation. In the current study, a mammalian expression platform was developed

which yields high quantities of correctly folded FimH, providing a path forward to manufacture sufficient quantities of FimH to enable clinical trials.

To address the relatively poor immunogenicity of FimH, we used a structure-based design strategy to engineer FimH proteins predicted to exhibit superior immunogenicity compared to the wild type (WT) protein. It has been suggested that locking $FimH_{LD}$ in the low affinity, 'open' conformation, induces the production of antibodies that can inhibit adhesion (36, 37). Conformational stabilization of antigens has been successful in improving immunogenicity and stability for various viral vaccine antigen candidates including Respiratory Syncytial Virus F protein (38-41). In this study, predicted conformationally stabilized FimH mutants were produced in mammalian cells and screened in a series of biochemical and biophysical assays followed by immunogenicity studies in mice. This screening approach led to the identification of a full length, donor strand-complemented FimH fusion antigen, FimH-DSG TM, which can be produced at a large scale in mammalian cells without a chaperone. By X-ray crystallography, we confirmed that the $FimH_{LD}$ of this mutant was stabilized in an open conformation, similar to its native presentation on pili.

Conformers can have quite different structures wherein the accessibility (or conformation) of epitopes in one conformer versus another differs (42). Therefore, depending on which conformer is used for immunization, immune responses (quality, magnitude, specificity) can differ significantly, as observed in this study. For this reason, it was important to understand the nature of the inhibitory Mabs elicited by the FimH-DSG adhesin.

Results:

Production of FimH in mammalian cells

The low yields of WT $FimH_{LD}$ or FimCH produced in *E. coli* are well documented (18, 19). Given these challenges, we explored production of FimH using an Expi293 mammalian cell expression system (**Fig. 1A**), wherein the protein is secreted into the cell culture medium using a eukaryotic signal peptide. Fusion of FimH to the mouse IgGκ signal peptide yielded protein that was correctly processed at the N-terminus (confirmed by mass spectrometry (data not shown)). Non-native N-linked glycosylation commonly occurs during heterologous expression of proteins in mammalian cells and can interfere with biological function as well as antigenicity of recombinant proteins. Non-native N-linked glycosylation on $FimH_{LD}$ at residues N7 and N70 was removed via mutation of target Asparagine residues to Serine, which was selected as a conservative substitution. WT and conformationally locked $FimH_{LD}$ (V27C L34C, described previously (19)), harboring N7S and N70S mutations to remove glycosylation, were expressed in 20 ml Expi293 cultures, which yielded 17 mg and 10.8 mg protein respectively.

Mammalian and *E. coli* derived $FimH_{LD}$ WT and V27C L34C were further characterized using biophysical and biochemical assays. The *E. coli* and mammalian derived $FimH_{LD}$ WT and mutant proteins had essentially identical near-UV circular dichroism (CD) spectra (**Fig. 1B**), indicating that tertiary structure of these proteins is very similar. Ligand binding affinity was determined using a direct binding fluorescence polarization (FP) assay with a fluorescein-conjugated octylbiphenylmannopyranoside (BPMP) ligand as described previously (19, 43). *E. coli* and mammalian produced material bound BPMP ligand with similar affinity (**Fig. 1C**); thermal stability, as determined by differential scanning calorimetry, was also comparable (**Fig. 1D**).

Design of a full-length donor strand complemented FimH (FimH-DSG)

To mimic the presentation of FimH on the assembled fimbrial tip (20), and understand the contribution of $FimH_{PD}$ in ability to elicit anti-FimH antibodies with the ability to prevent bacterial binding to mannose, we considered production of a full length FimH antigen. Full length FimH cannot be produced in *E. coli* without the chaperone FimC or as part of a pilus (16, 19, 44, 45). In previous studies in humans and non-human primates, full length FimH in complex with FimC was used as an immunogen (23-25, 33, 34). Whether the $FimH_{PD}$ is important for optimal immunogenicity is unknown, therefore the design of a full length FimH was explored to compare immunogenicity with that of $FimH_{LD}$ alone. Sauer *et al* previously produced a stable, isolated FimH molecule by displacing FimC in FimCH with a FimG donor strand peptide (FimG residues 1-14) (46). This approach requires coexpression of FimH with the chaperone, FimC. In contrast, Barnhardt *et al* produced a stable, single chain FimG donor strand complemented FimH in *E. coli* using a 4-residue amino acid linker (DNKQ), enabling production of full length FimH without a chaperone (17). The single chain concept was explored further in the current study. Donor-strand complemented, full-length FimH proteins (FimH-DSG) were produced by attaching a 14-mer donor strand peptide from FimG to the C-terminus of the $FimH_{PD}$ via a Glycine-Serine linker of various lengths, as well as the previously described DNKQ linker (17). Flexible polypeptide linkers consisting of Glycine and Serine are often used in construction of multidomain proteins as these flexible and hydrophilic spacer sequences prevent formation of secondary structure between protein domains, reducing the possibility that linkers will interfere with the folding or function of the target protein (47). Constructs were screened in mammalian cells and expression levels were similar, as assessed by SDS-PAGE (**Fig. S1**). FimH-DSG with a 7-residue Glycine-Serine linker (GGSSGGG) was selected based as optimal based on structural analysis. Non-native glycosylation in $FimH_{LD}$ was prevented by incorporation of N7S and N70S mutations as described above and an

additional mutation to Serine was also introduced at N228 in the $FimH_{PD}$. Analysis by mass spectrometry confirmed that FimH-DSG retained a single glycosylation site at N235 in the exploratory antigen characterized in this study (data not shown). Note, fully aglycosyl variants of FimH-DSG were subsequently generated following introduction of an additional N235S mutation and expression in ExpiCHO cells (described in brief below).

The proposed mechanism of action of FimH-containing vaccines to prevent UTIs is via inhibition of bacterial binding to the urinary tract epithelium (25). We developed a live, whole *E. coli* binding inhibition assay to quantify the ability of anti-FimH antibodies to prevent binding of fimbriated bacteria to a mannosylated surface (mimicking the mannosylated FimH receptor on the surface of bladder epithelial cells), based on previous work (48). Using this assay, the relative ability of *E. coli* and mammalian derived FimH proteins to elicit inhibitory antibodies in mice was evaluated (**Fig. 1E** and **Fig. 1F**). Inhibitory titers elicited by *E. coli* and mammalian derived WT $FimH_{LD}$ proteins in mice were equivalent, although the potency of the stabilized lock mutant $FimH_{LD}$ V27C L34C produced in mammalian cells was slightly lower than that of the *E. coli* produced $FimH_{LD}$ V27C L34C. Disulfide bond formation may differ in the periplasm of *E. coli* compared to the mammalian cytoplasm (49). Inhibitory titers elicited by full length FimH proteins (FimH-DSG, only produced in mammalian cells) including the previously described FimCH protein (50) were markedly higher than $FimH_{LD}$ proteins in terms of percentage of responders and geometric mean IC_{50} values (**Fig. 1F** and **Table S1**).

Rational design of FimH variants stabilizing the low-affinity, open conformation

We employed *in silico* analysis to identify novel variants predicted to stabilize $FimH_{LD}$ in a low affinity conformation, which is unable to bind its cognate mannose receptor. Crystal structures of

FimH in complex with fimbrial structural proteins in the absence of ligand or presence of D-mannose are shown in **Fig. 2A**, illustrating the differences in $FimH_{LD}$ conformation. The crystal structure of full length FimH in complex with fimbrial structural proteins (PDB ID 3JWN (20)) was used as a model. Suggested amino acid substitutions identified from this analysis were introduced into either $FimH_{LD}$ or FimH-DSG **(Fig. 2B**). To stabilize $FimH_{LD}$ in an open conformation, the following design strategies were applied: 1) nonpolar residues exposed to solvent in the pre-bound state but buried within the protein interior in the bound structure were mutated to polar or charged residues, disfavoring the high-affinity, closed conformation of $FimH_{LD}$, 2) disulfide linkages were introduced between residue pairs in close proximity in the pre-bound state, but not in the bound conformation, 3) mutation of glycine residues having a backbone F-angle < 0° in the pre-bound state but > 0° in the bound structure to prevent closure of the ligand binding site, 4) a full length, single chain FimH-DSG was designed (described above) 5) cavity filling mutations designed to stabilize the interface between $FimH_{PD}$ and $FimH_{LD}$ were introduced separately into full length FimH-DSG.

Screening of $FimH_{LD}$ and FimH-DSG mutants in *in vitro* assays

Sixty-four mutant and WT versions of $FimH_{LD}$ and FimH-DSG proteins were expressed in Expi293 cells as described above. Purified proteins were evaluated in a series of *in vitro* and *in vivo* studies (**Fig. 3A**). Mutants that were expressed at low levels were excluded from further evaluation. Binding affinities (K_d) of FimH mutants for mannoside ligand were determined by FP assay using BPMP as described above. K_d values for a subset of $FimH_{LD}$ and FimH-DSG mutants relative to WT are shown in **Fig. 3B** (data for additional mutants can be found in **Table S2**). The sequence of $FimH_{LD}$ WT is derived from *E. coli* UTI isolate J96 (51). V27A is a natural variant

that is associated with virulent UTI isolates and those associated with Crohn's Disease (11, 52). Introduction of the single point mutant V27A did not alter mannoside ligand binding affinity relative to $FimH_{LD}$ WT, while combining single or double glycine loop mutations at G15 or G16 positions with V27A significantly impaired ligand binding (**Table S2**). Ligand binding was completely lost in the triple mutant, $FimH_{LD}$ G15A G16A V27A ($FimH_{LD}$ TM, K_d > 2000 nM). Ligand binding affinity of FimH-DSG WT was reduced more than 100-fold compared to $FimH_{LD}$ WT, in agreement with the allosteric role of the pilin domain in regulating ligand binding by the lectin-binding domain. FimH-DSG V27A also had a two-fold lower ligand-binding affinity, compared to FimH-DSG WT (**Table S2**). This is consistent with previous data showing that a FimH mutant containing A27 has the propensity to adopt a less-active state that binds mannose with low affinity (11). Like $FimH_{LD}$, FimH-DSG mutants containing V27A and Glycine loop mutations have substantially reduced ligand binding activity. Altogether, our data suggest that the flexible Glycine loop plays a stabilizing role in ligand binding. Mutations in this loop result in FimH adhesins with poor affinity for the synthetic BPMP ligand used as representative of cognate mannosylated host cell glycoprotein receptors.

To further evaluate ligand binding abilities of FimH variants, a SYPRO orange-based differential scanning fluorimetry assay was used (19). The temperature at which 50% of the protein is unfolded (T_m) was determined for all mutants in apo state as well as in the presence of methyl alpha-D-mannopyranoside, a derivative of alpha-D-mannose that binds to FimH with micromolar affinity (53). The T_m of apo protein and its corresponding T_m shift (ΔT_m) in ligand bound condition are summarized in **Table S3**. FimH-DSG WT proteins exhibited significantly higher T_m (71.7 ºC) compared to $FimH_{LD}$ WT (61.5 ºC). T_m shifts of the FimH mutant proteins from apo to mannoside ligand bound conditions are in concordance with the changes seen in mannoside ligand K_d

measurement (**Fig. 3B, Table S2**). Of note, consistent with published data the V27C L34C disulfide lock mutant (19) exhibited significantly lower thermostability (T_m) compared to $FimH_{LD}$ and FimH-DSG WT proteins, while retaining mannoside ligand binding activity (Kd of 30-60 nM). In contrast, combinatory mutations containing V27A and Glycine loop mutations at G15 and G16 positions resulted in FimH mutants that retained thermostability while losing their ability to bind mannoside ligand (Kd >2000nM). Together with our binding affinity data, these data suggest that combining V27A and Glycine loop mutations stabilizes FimH proteins in a low affinity state that is largely incapable of ligand binding.

In previous work, WT and conformationally locked $FimH_{LD}$ mutants were found to have distinct tertiary structures (19). The secondary and tertiary structures of selected $FimH_{LD}$ and FimH-DSG proteins were therefore examined by CD (**Fig. S2**). The far-UV CD spectrum (secondary structure) of $FimH_{LD}$ WT expressed in mammalian cells is consistent with previously published data. Overall, the secondary structures of the $FimH_{LD}$ or FimH-DSG mutants are highly similar to WT proteins (**Fig. S2A**), suggesting that the overall secondary structure is not altered in these mutants. The near-UV CD spectra (tertiary structure) of most $FimH_{LD}$ mutants except for V27A (**Fig. S2B**), however, were quite different from that of $FimH_{LD}$ WT and are more similar to the previously reported $FimH_{LD}$ V27C L34C and V27A R60P mutants which assume an open conformational state (19). On the other hand, all FimH-DSG proteins including WT and the V27A, G15A, G16A triple mutant (or TM) had highly similar secondary and tertiary structures, resembling the open state of $FimH_{LD}$ (**Fig. S2**). Overall, the CD characterization is consistent with mannoside ligand binding data described above, which suggests these mutants are stabilized in an open conformation that has low mannose binding affinity.

Together, these data suggest that the Glycine loop mutations constrain $FimH_{LD}$ in an open conformation, while the FimH-DSG constructs including the corresponding reference WT variant, remain in a conformation that remains unchanged upon introduction of stabilizing mutations that eliminate ligand binding.

FimH-DSG mutants induce antibodies with superior ability to inhibit bacterial binding than $FimH_{LD}$ mutants in mice

To evaluate the relative ability of selected FimH mutants to elicit inhibitory antibodies, mice were vaccinated with each mutant protein and the collected sera were used to assess the ability to prevent bacterial binding *in vitro*. Mice were immunized three times with 10 µg FimH protein combined with QS21 adjuvant (**Fig. 4A**) and sera from post dose 2 and 3 time points were evaluated in the yeast mannan *E. coli* binding inhibition assay described above (**Fig. 4B** and **Table S6**).

At post dose 3, mice immunized with novel stabilized $FimH_{LD}$ mutants G15A G16A V27A, G16A V27A, and the previously described mutant V27A R60P (19) had higher responder rates and increased binding inhibition ($p < 0.05$) compared to $FimH_{LD}$ WT (**Fig. 4B** and **Table S6**). Other $FimH_{LD}$ mutants (G15A V27A, G16P V27A, V28C N33C) did not significantly enhance functional immunogenicity of $FimH_{LD}$. Thus, several mutants designed to enhance functional immunogenicity of $FimH_{LD}$ by constraining $FimH_{LD}$ in an open conformation led to improved responses relative to $FimH_{LD}$ WT, confirming previous findings (54). Following vaccination with 2 doses of $FimH_{LD}$ and FimH-DSG proteins, significantly more animals yielded inhibitory titers in the groups vaccinated with FimH-DSG compared to $FimH_{LD}$ (**Fig. 4B** and **Table S6**). This trend was sustained at PD3, where 95%-100% of mice responded in groups vaccinated with FimH-DSG V27A, FimH-DSG G15A V27A or FimH-DSG TM and tended to have higher GMC IC_{50} values

relative to $FimH_{LD}$ mutants ($p<0.05$) (**Fig. 4B** and **Table S6**). In conclusion, FimH-DSG mutants elicit higher inhibitory antibody responses compared to $FimH_{LD}$ mutants.

The ability of FimH-DSG V27A, G15A V27A and the G15A G16A V27A triple mutant (TM) to elicit inhibitory antibodies were similar. However, during large scale purification of FimH-DSG WT and TM from ExpiCHO cells for further characterization, a tendency for aggregation was observed for FimH-DSG WT and characterization by analytical size exclusion chromatography revealed the presence of high molecular weight complexes (**Fig. S3A-C**). We hypothesized that during CHO fermentation and upon secretion into the culture media the FimH-DSG WT binds glycan molecule(s) released from the surface of the host CHO cells. To evaluate this further, samples were analyzed by High pH Anion-Exchange Chromatography with Pulsed Amperometric (electrochemical) Detection (HPAEC-PAD). FimH-DSG WT preparations contained numerous monosaccharides (**Fig. S3D)**. In contrast, FimH-DSG TM was bound to comparatively fewer glycan moieties (**Fig. S3D**). Furthermore, it is entirely possible that the low monosaccharide content that was detected represents sugar moieties of the N-glycan present on N235. FimH-DSG TM did not tend to aggregate or form high molecular weight complexes. Therefore, as it can be purified to homogeneity, at a high yield, we used this mutant for our subsequent studies.

Production of aglycosylated FimH-DSG TM

Removal of the N-glycan present on residue N235 of FimH-DSG TM led to additional glycosylation on residue N228. To avoid these issues, we explored removal of glycosylation by introducing the following combinations of mutations: N228S N235S, T230A T237A, N228G N235G, and N228Q N235Q. Proteins were expressed transiently in 2L ExpiCHO cell cultures and yields were between 69 mg (N228G N235G) and 311 mg (N228S N235S). Aglycosylation

mutations did not impact the ability of inhibitory Mabs to bind relative to glycosylated FimH-DSG TM (**Table S7**), and the capability of aglycosylated variants elicit adhesin blocking antibodies does not appear to differ from the glycosylated parent (**Fig. S4**).

Structural characterization of FimH-DSG TM by X-ray Crystallography

Among all conformationally stabilized FimH-DSG mutants, FimH-DSG TM was of most interest as it harbors the two Glycine loop mutations G15A and G16A designed to conformationally lock the mannose site in the 'open' state. To verify the conformation of FimH-DSG TM, the crystal structure of a FimH-DSG TM protein containing four glycosylation site mutations (N7S, N70S, N78S, and N228Q) was solved by X-ray crystallography at 1.9 Å resolution (**Fig. 5A** and **Table S9**). There are four molecules of FimH-DSG TM in one asymmetric unit which share high similarity, therefore, structural analysis was done with protomer A. Introduction of the glycosylation site mutations did not appear to alter either the local or global conformations of the $FimH_{LD}$ and $FimH_{PD}$. Comparison of the structure to previously determined structures of $FimH_{LD}$ confirmed that FimH-DSG TM lectin domain adopts a compressed structure with an open mannose-binding pocket (**Fig. 5C**). Clear electron density was obtained for the Glycine loop, wherein the G15A G16A mutations were introduced which induced a local change in the loop conformation (**Figs. 5B, 5C**). A15 projects towards the inside region of the clamp loop, providing rigidity, which causes the loop to widen at the end by ~1.2 Å (Ile13 Ca-Ser17 Ca) compared to the WT residue (G15), thus stabilizing the low affinity state. Additional ridigity is introduced by the G16A substitution, as it projects towards the bulk solvent. By comparison, these residues adopt very different conformations in the closed, high-affinity state (55). The overall structure of FimH-DSG TM resembles the low affinity conformation of $FimH_{LD}$ (**Fig. 5D**) (16, 18). In comparison to previously published structures, the donor strand complemented $FimH_{PD}$ did not exhibit any

conformational changes. The backbone of the exogeneous 7-residue Glycine-Serine linker that connects the FimH and FimG peptide could largely be resolved, and does not impact on the conformation of the lectin or pilin domains in comparison to previously published structures (**Fig. S5**) (18).

Inhibitory antibodies elicited by FimH-DSG map to novel epitopes

As described above, FimH-DSG WT and derived mutants induced superior inhibitory antibody responses in mice compared to equivalent $FimH_{LD}$ variants. To further characterize inhibitory antibodies induced by FimH-DSG, monoclonal anti-FimH antibodies were developed and screened by the yeast mannan *E. coli* binding inhibition assay, which resulted in the identification of 10 unique clones (**Table 1)**.

A series of competition experiments using Bio-layer interferometry (BLI) was undertaken to facilitate Mab classification and epitope mapping. As comparators, two previously described inhibitory Mabs, 475 and 926, which bind to overlapping epitopes on the ligand binding interface, were included (48, 54). Experiments were performed with and without octylmannopyranoside ligand, to assess whether there is competition between the ligand and Mab binding to $FimH_{LD}$ (**Table 1, Fig. S6)**. These experiments identified four distinct inhibitory epitopes. Site 1 was recognized by 6 novel Mabs, as well as reference Mabs 926 and 475, which effectively block ligand binding. Three Mabs were unable to block ligand binding and bound to two distinct epitopes (site 2 and site 3, composed of 327-3 and 329-2, and 445-3 respectively). Site 4 was recognized by a single Mab (440-2) that bound exclusively to conformation-stabilized $FimH_{LD}$. Note, this Mab was derived from mice immunized with the conformationally locked construct, FimH-DSG

V27C L34C. Individual Mab binding kinetics are shown in **Table 1** alongside their inhibitory concentrations in the *E. coli* binding inhibition assay.

Fab fragments derived from representative antibodies from each new site (329-2 (site 2), 445-3 (site 3) and 440-2 (site 4)) were selected as representatives for subsequent epitope mapping by cryo-EM. The small size of FimH was an impediment to high resolution structural analysis of FimH-Fab binary complexes, which yielded only low-resolution structures that could not be modeled. To circumvent this limitation, a combinatorial approach was taken in which pairs of Fabs with non-overlapping epitopes were combined with FimH to form ternary complexes, increasing the overall particle mass to 125 kDa. Using this ternary complex strategy, a cryo-EM structure of FimH-DSG TM with Fabs 329-2 and 445-3 was determined at 3.11 Å (**Fig. 6A, Fig. S7, Table S10**), with the final map comprising $FimH_{LD}$ and the antigen-binding portions of each Fab, allowing molecular modeling of each component and identification of the molecular details of the respective epitopes. The two Fabs were distinguished in part by comparison of their sequences to the side chains in the map, but to build additional confidence, the structure of a similar FimH-DSG TM ternary complex, in which the 329-2 Fab was replaced with 440-2, was determined by cryo-EM (**Fig. 6B, Fig. S8, Table S10**). While the new map from a 3.9 Å reconstruction could be used to identify density corresponding to FimH and both Fabs, the map resolution and quality were limited by under-represented particle views, allows only rigid body fitting of models. Comparison of the Fab positions in both structures, however, confirmed the Fab assignments for 329-2 and 445-3, and further allowed mapping of the 440-2 epitope. Surprisingly, Mab 440-2 binds to the tip of $FimH_{LD}$, which covers the mannose binding site and largely overlaps with the known site 1. Binding of Mab 440-2 (site 4) therefore directly competes with mannose binding, conveying an orthosteric inhibition mechanism for blocking of bacterial adhesion, like that observed for the

competitive Mab 475 (48). However, being derived from a conformationally locked FimH-DSG mutant distinguishes Mab 440-2 from other inhibitory Mabs. Mab 440-2 preferentially binds to the low affinity open state of $FimH_{LD}$, but not WT $FimH_{LD}$ (**Table S4**), suggesting that it uses a novel inhibitory mechanism. Indeed, the structure of the ligand binding site of 440-2-bound $FimH_{LD}$ matches the open conformation, largely distinct from the observed conformation in the ligand bound high-affinity 'closed' state (**Fig. 7A**).

External to the ligand binding site, epitopes of Mabs 329-2 (site 2) and 445-3 (site 3) were mapped to the opposite sides of $FimH_{LD}$. Despite not overlapping with ligand binding pocket, the 329-2 and 445-3 epitopes are composed of residues from the flexible loops that are part of the ligand binding site, with conformations that change significantly during the switch between inactive and active states. In particular, Mab 329-2 recognizes a novel inhibitory epitope comprised of residues T5, S7, T9, A10, Y21 and N23. These residues are connected to the Glycine loop that harbors the G15A and G16A mutations. As a result, binding of Mab 329-2 stabilizes the Glycine loop in the open conformation that has low mannose affinity (**Fig. 7B**). Binding to the other side of $FimH_{LD}$, Mab 445-3 interacts with residues including R132, T134, S139, D140 and D141 from the clamp loop in its open conformation, which shifts 4.4 Å away from the compact-mannose-bound conformation seen in the closed form (PDB ID 6GTV, **Fig. 6B**). In addition, S80, S81, Y82 and P91 were also mapped to 445-3 binding site. These residues were revealed in previous work as being part of a critical epitope for Mab 824, an inhibitory antibody that allosterically prevents transitions of FimH from low-affinity to high-affinity states (56). Taken together, Mab 445-3 likely blocks bacterial adhesion via a combinatory allosteric mechanism which modulates both the global state transition as well as the local ligand binding site. These new epitopes described herein, along

with previously identified FimH Mab epitopes are highlighted on the structure of FimH-DSG TM in **Fig. 6C**.

Of note, none of the epitopes mapped for these three Fabs overlap with the conformation stabilizing mutations introduced into the FimH-DSG TM vaccine candidate. Collectively, these results broaden the repertoire of $FimH_{LD}$ functional epitopes, highlighting the diverse interference mechanisms by which antibodies contribute to FimH vaccine efficacy.

Discussion:

FimH is a key target for UTI vaccines due to its integral role in UPEC virulence. However, clinical trials have yet to demonstrate a clear protective effect of FimH immunization in humans (33). As there are issues with scalable production and poor immunogenicity documented in previous studies, we sought to optimize the antigen design and how it is bioprocessed to improve its application for therapeutic use.

Firstly, we developed a mammalian expression system to produce FimH antigens. In contrast to classic osmotic shock approaches that release functional FimH from the *E. coli* periplasm, the mammalian expression platform dramatically increases yield and simplifies the purification process. Notably, FimH antigens produced in mammalian cells are structurally and antigenically alike to the analogous proteins produced in *E. coli*. Our approach provides a path forward for manufacture of FimH antigens in large quantities for clinical trials and may be applicable to other complementary fimbrial vaccine antigens, that are similarly expressed at low levels in *E. coli*.

Computational design has been used successfully to optimize vaccine antigens for improved stability, immunogenicity (57, 58) as well as safety (57, 59, 60). The design of

conformationally stabilized proteins to improve neutralizing responses was pioneered in the field of respiratory syncytial virus (RSV) research (38) and has been employed for COVID-19 (39), HIV (40), influenza (41), and malaria vaccines (61). In agreement with previous reports (54) our rational approach to engineering structurally constrained FimH mutants led to identification of an conformation-stabilized full-length FimH variant (FimH-DSG TM) that elicits superior bacterial binding inhibition when compared to WT or conformation-stabilized mutants of $FimH_{LD}$. $FimH_{PD}$ is thought to act as an allosteric inhibitor of the $FimH_{LD}$ and interaction of $FimH_{LD}$ with $FimH_{PD}$ in full length FimH stabilizes the $FimH_{LD}$ in the low-affinity state (62). Similarly, full length FimH-DSG TM is stabilized in the low affinity state (**Fig. 5**). Introduction of conformation stabilizing mutations (*e.g.,* G15A, G16A, V27C L34C) into FimH-DSG did not dramatically impact binding affinity nor immunogenicity further. As no inhibitory Mabs were found to bind $FimH_{PD}$ in screening of FimH Mabs, the $FimH_{PD}$ thus likely contributes to the increased immunogenicity of FimH-DSG compared to $FimH_{LD}$ mutants via stabilization of the $FimH_{LD}$ conformation. We hypothesize that this effect is due to exposure of binding pocket epitopes in the open conformation, enabling targeted antibody development against prebound FimH. Like other allosteric proteins, FimH can adopt different conformations, which, in turn, can affect accessibility and structure of functional (inhibitory) epitopes. Thus, different $FimH_{LD}$ conformations may be antigenically distinct, and induce immune responses that differ in specificity or inhibitory function. This is well-documented for several viral proteins, including RSV fusion protein F: immunization with the prefusion-stabilized conformer induces a more potent neutralizing antibody responses, unlike the responses induced by the postfusion form(38). Similar observations have been made for SARS-CoV-2 Spike protein (63) and HIV-1 envelope protein (64).

Characterization of inhibitory Mabs elicited by FimH-DSG by epitope binning and cryo-EM revealed three non-overlapping epitopes present on $FimH_{LD}$; indicating that inhibitory antibodies targeting FimH-DSG TM can act via more than one mechanism. Based on the characterization of antibodies raised against $FimH_{LD}$, three types of FimH inhibitory antibodies are described in the literature (48, 62): orthosteric (where an antibody replaces ligand in the binding site), parasteric (where an antibody binds adjacent to ligand in the binding site), or dynasteric (where the antibody binds at an allosteric site distant to the ligand binding site, preventing a conformational switch). The analysis described herein mapped antibodies to the ligand binding site (site 1), as described previously, and three novel sites (sites 2, 3 and 4) that represent alternative novel allosteric mechanisms by which FimH directed antibodies can inhibit binding.

In addition to the improvements in immunogenicity and induction of antibodies against novel inhibitory epitopes, the single chain FimH-DSG TM antigen presented herein offers several advantages over existing FimH protein vaccine candidates. Production of FimH-DSG in mammalian cells yielded high levels of protein, which induced potent inhibitory titers in sera from immunized mice. FimH-DSG mimics the natural presentation of FimH in the context of the assembled pilus, without the need for a chaperone, resulting in a targeted immune response. Introduction of the three stabilizing mutations (G15A G16A V27A) enabled purification to homogeneity without copurification of contaminating glycans compared to WT FimH-DSG. The ability to express a fimbrial adhesin in mammalian cells at high yield, to homogeneity, in a highly immunogenic form, represents a key advancement in the production of fimbrial antigens for effective vaccine development.

Conclusion:

472 UTIs are a common problem and a primary source of sepsis in the immunocompromised and
473 elderly (65). A vaccine which can decrease UTI may ultimately decrease rates of hospitalization
474 and sepsis-associated morbidity and mortality. The optimized, highly immunogenic full length
475 FimH antigen described in this study can be produced at scale in mammalian cells and induces
476 potent inhibitory antibodies that have novel mechanisms of action. Thus, FimH-DSG TM is a
477 promising candidate to evaluate further in efficacy studies against FimH-expressing *E. coli*.

478

Materials and Methods:

Experimental Design

This work aimed to develop a *E. coli* vaccine candidate by applying a computational and experimental design strategy to enhance the stability of the FimH lectin binding domain ($FimH_{LD}$) and single chain full length FimH (FimH-DSG). Mutations were designed to introduce amino acid substitutions in $FimH_{LD}$ to stabilize the protein conformation in a low affinity state. $FimH_{LD}$ and FimH-DSG mutants were expressed in mammalian cells and purified mutant proteins were characterized by thermal stability and rate of dissociation, in comparison to wild type $FimH_{LD}$. The crystal structure of FimH-DSG G15A G16A V27A (FimH-DSG TM) was resolved to confirm the mutant's open conformation. Monoclonal antibodies raised against FimH-DSG were evaluated in competition experiments to group into non-overlapping epitope bins. Representatives of each distinct bin were complexed with FimH-DSG TM and analyzed by Cryo-EM to determine epitopes.

Ethics statement

Mouse immunogenicity studies were performed at Pfizer, Pearl River, NY, which is accredited by the Association for Assessment and Accreditation of Laboratory Animal Care (AAALAC). All procedures performed on mice were in accordance with local regulations and established guidelines and were reviewed and approved by an Institutional Animal Care and Use Committee (IACUC). The work was in accordance with United States Department of Agriculture Animal Welfare Act and Regulations and the NIH Guidelines for Research Involving Recombinant DNA Molecules, and Biosafety in Microbiological and Biomedical Laboratories.

Expression and purification of WT $FimH_{LD}$ from *E. coli*

DNA encoding J96 $FimH_{LD}$ sequence was cloned into a pET28 vector and *E. coli* BL21(DE3) cells were transformed with the resulting construct. Expression, extraction and purification of $FimH_{LD}$ or FimCH from the *E. coli* periplasm was performed as previously described (50, 66).

Expression and purification of WT FimH and mutants in mammalian cells

DNA encoding J96 FimH sequence and its mutants was codon optimized for mammalian cells and cloned in frame behind sequence encoding mouse IgGκ or native FimH signal peptide, along with a C-terminal 8xHis tag in pcDNA3.1(+). FimCH was expressed from a pBudCE4.1 plasmid containing a CMV promoter to drive expression of FimC with a C-terminal 8xHis tag and a second promoter, EF1α, to drive expression of untagged FimH. For biochemical assays and mouse immunogenicity studies, endotoxin-free DNA was transiently transfected into Expi293 cells (ThermoFisher Scientific) according to manufacturer's instructions. Supernatants were filtered through a 0.22 μm filter unit (Nalgene sterile disposable filter with PES membranes, ThermoFisher Scientific). Nickel Sepharose excel (Cytiva) was incubated with supernatants overnight at 4ºC and purification was performed according to manufacturer's instructions. The eluate was loaded onto a S200 16/600 column in 50 mM TrisHCl pH 8.0, 300 mM NaCl. Fractions containing pure protein were pooled.

For X-ray crystallography and cryoEM, FimH-DSG TM was produced in ExpiCHO cells (Thermo Fisher Scientific) according to manufacturer's instructions. The purification procedure is described in the supplemental material.

525 **Computational design of FimH mutants stabilizing the native state**

526 The crystal structure of native full length FimH in complex with fimbrial structural proteins (PDB
527 ID 3JWN) was used as a model for the low-affinity, open conformation. The crystal structure of
528 $FimH_{LD}$ in complex with butyl α-D-mannoside was used as a model for the high-affinity, closed
529 conformation (PDB 1UWF). Schrodinger BioLuminate (release 2017-2) was applied to analyze
530 structural differences between the two states and to identify residue locations for mutations.
531 Nonpolar residues that are exposed to solvent in the pre-bound structure and buried in the bound
532 state were changed to polar or charged residues. Residue pairs selected for mutations to cysteine
533 to form disulfide bonds that stabilize the native state were proximate (C_β-$C_\beta \leq 5$ Å) in the pre-
534 bound state and distant (C_β-C_β ³ 10 Å) in the bound conformation. Gly residues that have a negative
535 backbone F-angle in the pre-bound state and a positive backbone F-angle in the bound state were
536 mutated to Ala or Pro. An optimal Gly-Ser linker to connect the C-terminus of FimH and the N-
537 terminus of FimG was identified using the Linker Modeler implemented in Molecular Operating
538 Environment (MOE v2018, Chemical Computing Group).
539
540 **Characterization of WT and mutant FimH proteins**
541 WT and mutant FimH proteins were characterized by fluorescence polarization, circular dichroism
542 and differential scanning fluorimetry modified from Rabbani et al (19) and are described in the
543 supplemental materials.
544
545 **Antigenicity assay**
546 Inhibitory Mabs 299-3, 304-1 and 440-2 (developed in-house) were used to confirm the
547 conformational state of FimH mutants; 299-3 and 304-1 bind to similar epitopes as Mab 475 and

926 (37, 48) while 440-2 recognizes a different epitope and appears to preferentially bind $FimH_{LD}$ in an open conformational state. Mutants that maintain the same structure as WT $FimH_{LD}$ are expected to bind all antibodies. Octet HTX from ForteBio was used for all the kinetic real-time biomolecular interaction experiments to measure antibody reactivity with each mutant. Experiments were carried out at 30 °C with 1000 rpm agitation in 96-well black plates containing 240 µl per well. Ni-NTA biosensors were equilibrated in buffer containing 1x PBS buffer containing 0.5 % BSA and 0.05 % Tween 20 (PBT) before allowing them to load his-tagged FimH mutant proteins at 5 µg/ml for 5 min. FimH loaded biosensors were allowed to reestablish baseline in PBT for 3 min before allowing them to associate with antibodies from different bins at 5 µg/ml for 5 min. Octet data analysis software was used for kinetic analysis of association step and obtain response in nm shift (tabulated).

FimH whole cell binding inhibition assays

CFT073 (ATCC) was serially passaged in 10 ml of Luria Bertani broth in static growth conditions at 37°C to enrich for FimH expression. Surface expression reaching ≥95 % was confirmed via flow cytometry using anti-FimH Mab 926 (48). Prior to the assay, 384 well white Maxisorp plates (Nunc) were coated with 20 µg/ml of yeast mannan (Sigma-Aldrich) and blocked in 1 % BSA (Thermo). FimH-expressing *E. coli* cells (confirmed by flow cytometry using an anti-FimH antibody) were then incubated with a titration of vaccinated mouse sera and controls. Sera were diluted in PBS + 0.1 % BSA and titrated 2.5-fold for 7 points, starting at 1:100. After 45 minutes at 37 ºC, the mixture was added to the plate and incubated for 45 minutes at 37ºC before washing away any unbound cells. A titration of anti-$FimH_{LD}$ rabbit sera was used as an internal control on every plate. Specificity of bacterial binding to mannan was established by the inclusion of Methyl

571 α-D-mannopyranoside (Sigma) as a negative control, which reduced binding by >95% at 50 mM
572 levels. Adherent cells were measured with a luminescent probe BacTiter Glo (Promega) and read
573 on a Clariostar Plus plate reader. IC_{50} inhibition values were interpolated using sigmoidal dose
574 response variable-slope curve fitting (Graphpad Prism). Titers are the reciprocal of the serum
575 dilution at which half-maximal inhibition is observed. Responders were defined as those with
576 ≥50% inhibition at the starting dilution, had a defined IC_{50}, a positive hillslope, r^2 ≥0.80 and at
577 least two points trending towards binding inhibition. The limit of detection (LOD) is designated
578 as a dilution of 50, which is half of the maximum dilution. The statistical significance (*p*-value)
579 of differences in responses between groups was determined using an unpaired t-test with Welch's
580 correction applied to log-transformed data.

581 An alternative version of the assay was used for only Figure 1 and involved detection using a
582 directly labelled anti-O25b-AF488 antibody and an O25b clinical *E. coli* isolate PFEEC0547
583 (collected as part of the ATLAS surveillance program).

584

585 **Animal studies**

586 Animal studies were conducted according to Pfizer local and global Institutional Animal Care and
587 Use Committee (IACUC) guidelines at an Association for Assessment and Accreditation of
588 Laboratory Animal Care (AAALAC) International-accredited facility.

589

590 **FimH murine immunogenicity studies**

591 6–8-week-old female CD-1 mice were obtained from Charles River Laboratories. For each group
592 of mice, 20 animals were immunized three times subcutaneously with 10 µg FimH protein mixed
593 with 20 µg Quillaja Saponaria-21 (QS-21) from a 5.1 mg / ml QS-21 stock solution containing 5

mM Succinate, 60 mM NaCl, 0.1% PS80, pH 5.6. Mice were bled 2 weeks following immunization. Blood was withdrawn in 3.5-mL serum tubes at each time point and spun in a centrifuge at 3,000 rpm for 10 min. The serum fractions were collected and stored in cryovials.

Anti-FimH Monoclonal antibody production

CD-1 mice immunized with purified WT FimH-DSG or FimH-DSG V27C L34C proteins in combination with QS21 adjuvant described above received a final intraperitoneal boost of 10 µg mixed with 20 µg QS21 FimH protein 4 days before fusions. Spleens cells from mice with high titers were harvested and fused with the myeloma P3X63-Ag8.653 cell line using polyethylene glycol (P7306, SIGMA HYBRI-Max). Fused cells were cultured in 96 well plates at 37 °C, 8 % CO_2 in DMEM containing HAT supplement (21060-017 Gibco). After 10 days in culture, hybridomas were screened by enzyme-linked immunosorbent assay (ELISA) using Maxisorp high binding 96 well plates (442404, Thermo Fisher Scientific) coated with 100 ng of FimH-DSG WT protein. Positive hybridomas secreting anti-FimH antibody were subcloned and clonality was assessed by sequencing. Over 300 parent hybridoma Mabs were screened for the ability to inhibit *E. coli* binding to yeast mannan using a single point titration assay. Following clonal expansion and competitive binding (binning) experiments (described in the supplemental material), 5 groups of antibodies with non-overlapping binding sites were identified.

FimH-DSG TM crystallization and structure determination

Purified FimH-DSG TM, with triple stabilizing mutations (G15A, G16A, V27A), aglycosylation mutations (N7S, N70S, N228Q), a 7-residue Gly-Ser linker, FimG donor strand peptide and a C-

terminal 8xHis tag, was buffer exchanged with 20 mM Tris (pH 7.5) using PD-10 column and concentrated to 10 mg/ml. Crystallization was performed at 20 °C using sitting drop vapor diffusion method by mixing equal volumes of protein and reservoir solution containing 1 M Sodium Acetate (pH 4.5) and 25% (w/v) PEG 3350. Crystals grew to their maximum size in ~7 days. Crystals were cryoprotected using the reservoir solution supplemented with 15% glycerol and flash frozen in liquid nitrogen. Diffraction data were collected at APS 17-ID. The data was processed using autoPROC (Global Phasing Limited) and the structure was solved using WT FimH-DSG complex (PDB code 4XOD) as a starting model. Model building and refinement were carried out using COOT (67) and BUSTER (Global Phasing Limited).

Characterization of ability of Mab to target ligand binding site

This experiment was conducted on OCTET HTX using Ni-NTA biosensors and buffer containing 1x PBS, 1 % BSA and 0.0 5% Tween 20. Two-fold dilutions (from 10 µg/ml to 0.078125 µg/ml) of Octyl-mannopyranoside ligand were prebound to 5 µg/ml of His-tagged $FimH_{LD}$ WT for 10 min. Biosensors were allowed to capture $FimH_{LD}$ WT prebound to ligand for 5 min. The baseline was established before letting the biosensors loaded with FimH and different concentrations of ligand allowed to bind 5 µg/ml FimH Mab for 5 min. Nanometer response of antibody binding obtained from each dilution of the ligand was plotted against ligand concentration.

Cryo-EM Sample Preparation, Data Collection, and Processing

637 For cryo-EM studies, Fab fragments of Mabs 299-3, 304-1, 329-2, 440-2 and 445-3 were generated
638 using one of two methods 1) using a Mouse IgG1 Fab and F(ab′)^2 Preparation Kit (Thermo
639 Scientific™ Pierce™) which uses immobilized Ficin for cleavage 2) production of recombinant
640 Fab fragments with a C-terminal his tag in ExpiCHO cells, by LakePharma. Cryo-EM sample
641 preparation, data collection and processing are described in full in the supplemental methods.

642 **Statistical analysis**

643 Statistical significance (*p*-value) of differences in responses between mouse groups was
644 determined using an unpaired t-test with Welch's correction, applied to log-transformed data.
645
646 **Acknowledgements:** Thank you to Elliot Dean and Lily Liu for molecular biology and thermal
647 shift support. Thank you to the Pfizer Pearl River Comparative Medicine group for their support
648 for animal studies. We thank and Andy Weiss for critical review of the manuscript. We thank
649 Christina D'Arco for scientific writing support.
650
651 **Author Contributions:** Conceptualization: YC, MCG, NCS, RGKD, LC
652 Methodology: LC, YC, SS, JL, JH, SK, MCG
653 Investigation: DK, LC, JL, CP, JA, TC, AI, SK, LL, AG, AE, JH, JM, CK, MK, KC, SS, MCG
654 Visualization: JJ, JL, HW, YC, NCS
655 Project administration: NCS, RGKD, ASA
656 Supervision: NCS, RGKD, YC, AA
657 Writing – original draft: NCS, LOC, YC
658 Writing – review & editing: HW, JJ, YVM, MCG, JL, JH, SK, CP, AE, LL, DK, JA, TC, AI, CK,
659 MK, KC, SS, AG, AA, RGKD

Financial disclosure statement: This work was supported by Pfizer Inc. Pfizer was involved in the study concept and design, the collection, analysis and interpretation of the data, the drafting of the manuscript, and the decision to submit the manuscript for publication.

Competing interests: All authors were employees of Pfizer Inc. during the conduct of this work and may hold Pfizer stock and/or stock options.

Data and materials availability: All data associated with this study are present in the paper or the Supplementary Materials.

673 **Figures**

674 **Fig. 1 FimH$_{LD}$ produced in mammalian cells has comparable biophysical properties to**
675 **material produced in *E. coli***

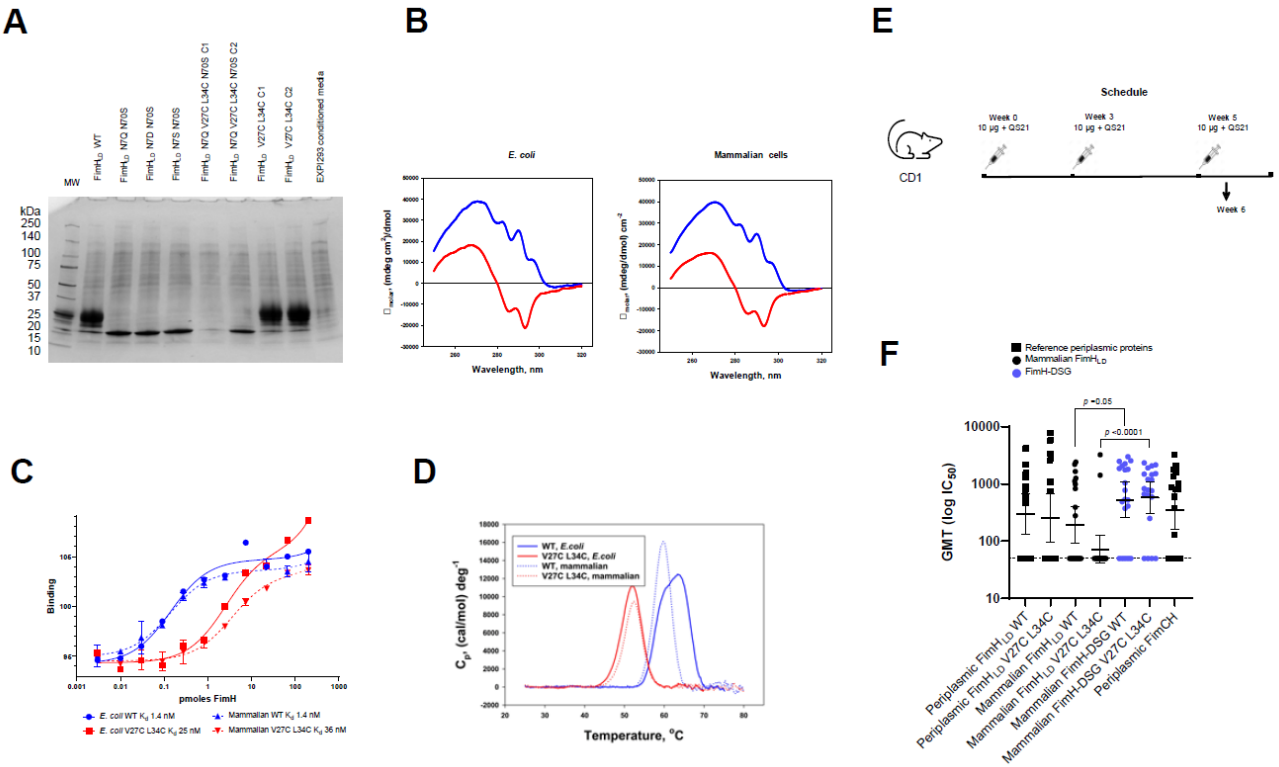

676

677 WT or conformation stabilized FimH$_{LD}$ were expressed in Expi293 cells along with mutants
678 designed to remove non-native glycosylation on residues N7 and N70. **(A)** Batch purified proteins
679 run on SDS-PAGE gel stained with Coomassie blue. C1 and C2 designate two clones of FimH$_{LD}$
680 N7Q V27C L34C N70S and FimH$_{LD}$ V27C L34C C1 that were evaluated for expression. (**B**).
681 Near-UV CD spectra of FimH$_{LD}$ produced in *E. coli* and mammalian expression systems. Spectra
682 of FimH$_{LD}$ WT (blue) and V27C L34C (red) are shown. **(C)** Affinity of WT and V27C L34C
683 FimH$_{LD}$ produced in *E. coli* or mammalian cells for alpha-D-mannopyranoside by FP. **(D)** Thermal
684 stability of WT and V27C L34C FimH$_{LD}$ produced in *E. coli* or mammalian cells. **(E)** Mouse study
685 design: CD-1 mice were immunized 3 times with 10 µg FimH proteins with QS21 adjuvant. **(F)**

686 Sera were analyzed for the ability to block FimH-expressing *E. coli* binding to yeast mannan; bars
687 represent geometric mean IC_{50} and 95% confidence intervals. Statistical significance (*p*-value) of
688 differences in responses between groups was determined using an unpaired t-test with Welch's
689 correction applied to log-transformed data; the bars and asterisk illustrate the significance of the
690 difference in response for comparisons.
691
692

693 **Fig. 2 Rational design of FimH mutations stabilizing the native state**

694

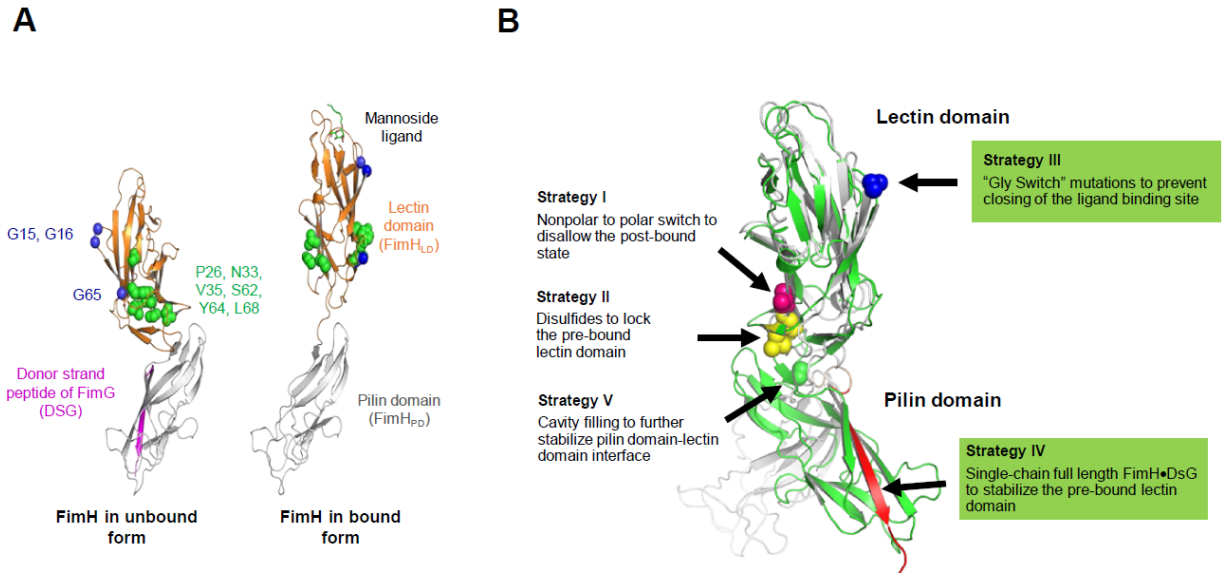

695

696 (**A**) Structures of FimH in unbound form (PDB structure 3JWN) and bound to mannoside ligand
697 (PDB structure 1KLF). In pili, unbound FimH (left), complexed with the donor strand of FimG,
698 adopts a compact conformation that binds the FimH cognate receptor, the terminal mannose
699 moiety of glycosylated proteins, with low affinity. Upon binding a mannose moiety (right), the
700 $FimH_{LD}$ and $FimH_{PD}$ separate, sidechains (colored in green) flip from protein interior to surface,
701 and backbones of Gly residues (colored in blue) exhibit large conformational changes. Residues
702 shown in blue and green were targeted for mutagenesis. **(B)** Strategies employed to stabilize FimH
703 conformation. Unbound (grey) and bound (green) full length FimH structures with residues
704 targeted by mutagenesis are highlighted.

705

Fig. 3 Identification of FimH mutants with improved thermal stability and reduced mannoside ligand affinity

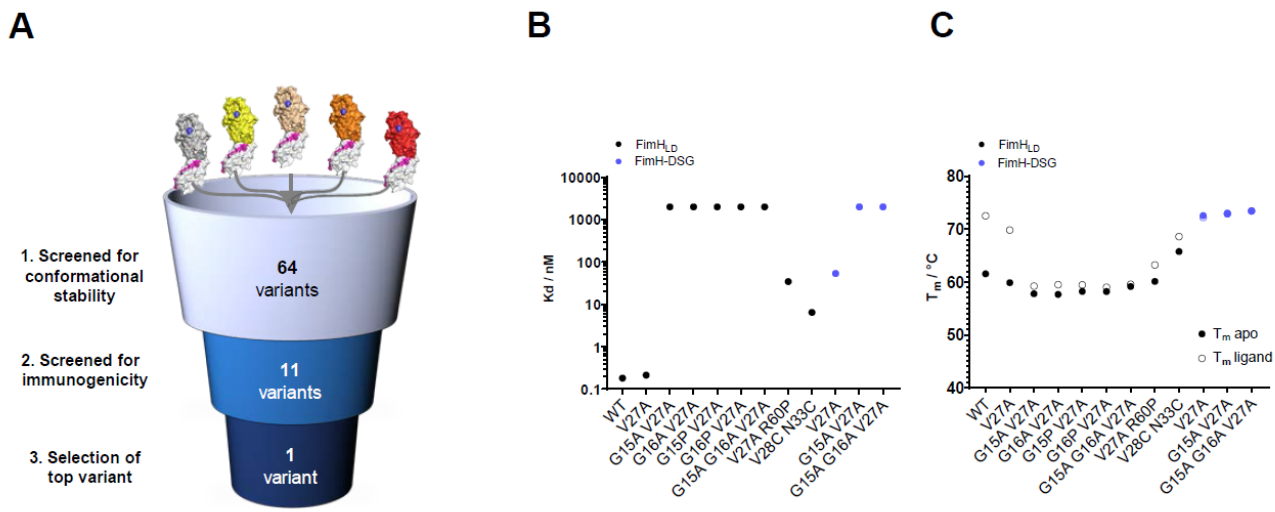

(A) 64 FimH variants were screened *in vitro* for ability to bind mannose, thermal stability, and conformation. A subset of constructs was screened for immunogenicity in mice. **(B-C)** Biochemical characterization of purified $FimH_{LD}$ and FimH-DSG mutants. **(B)** relative average binding affinities of FimH mutants to mannoside ligand. Note, the assay limit of detection was ~2000 nM. **(C)** filled circles display average melting temperatures of each mutant. Open circles denote melting temperature of FimH protein in the presence of mannoside ligand. Tabulated K_d and T_m values for all mutants are in **Tables S2** and **S3** respectively.

Fig. 4 FimH-DSG mutants induce antibodies with superior ability to inhibit bacterial binding compared to $FimH_{LD}$ mutants in mice

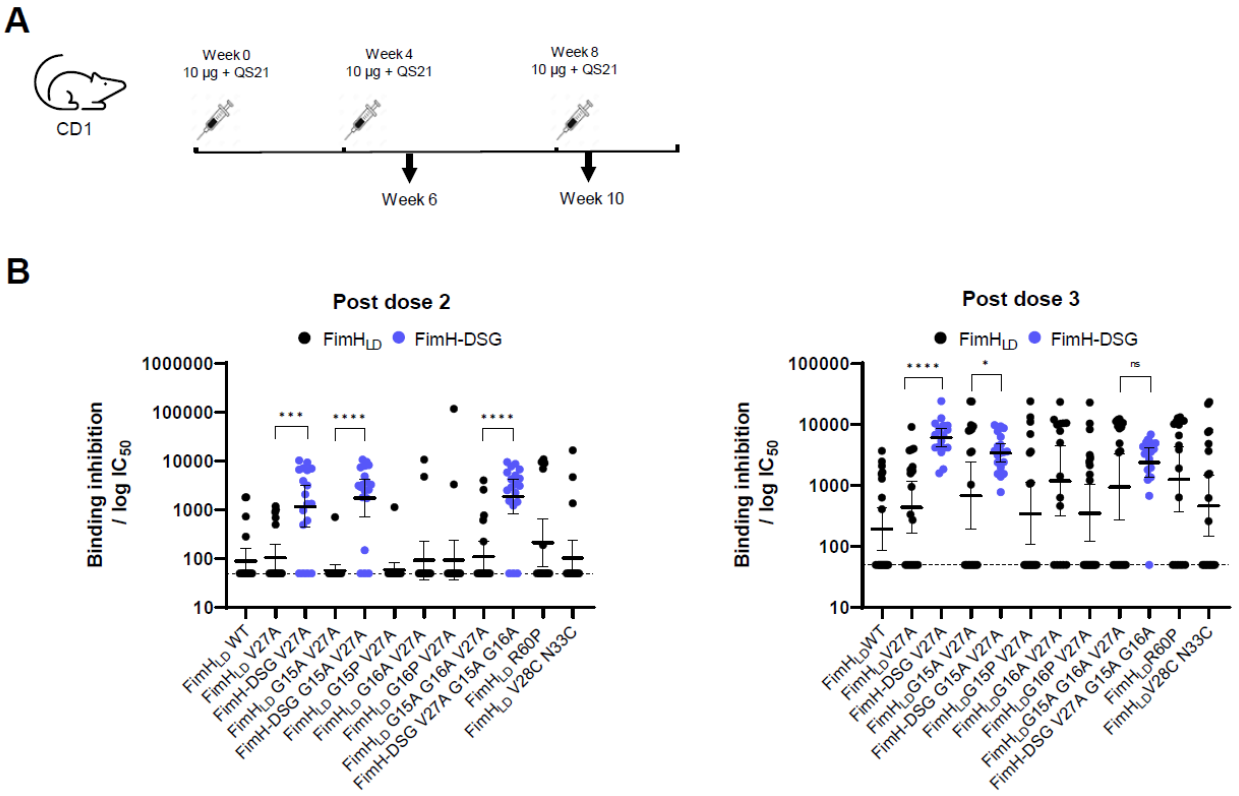

(A) CD-1 mice were immunized 3 times with 10 µg FimH with QS21 adjuvant. Sera were analyzed for the ability to block FimH-expressing *E. coli* binding to yeast mannan. **(B)** Inhibitory titers were determined from serial dilution of sera from vaccinated mice and represent the reciprocal of the dilution of serum at which 50% of bacteria remain bound to the plate and are shown for post dose 2 and post dose 3 timepoints. Statistical significance (*p*-value) of differences in responses between groups was determined using an unpaired t-test with Welch's correction applied to log-transformed data; the bars and asterisk illustrate the significance of the difference in response between groups. Tabulated IC_{50} values are shown in supplemental **Table S6**.

730 **Fig. 5 The lectin domain of FimH-DSG TM adopts an open conformation.**

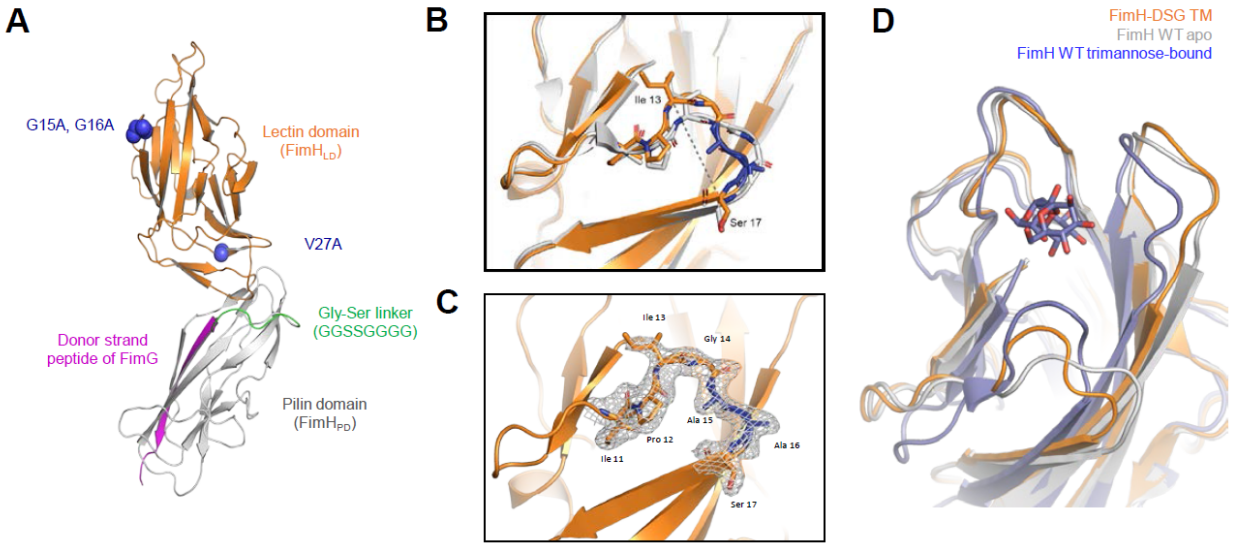

731

732 **(A)** Overall structure of FimH-DSG TM from x-ray crystallography data (PDB code 8V3J). **(B)**
733 Superimposition of ligand binding sites of FimH-DSG TM (orange) and WT FimH from a
734 previously published structure of native pili (PDB code 3JWN, light grey) shows remodeling of
735 the Glycine loop due to G15A G16A mutations. The widening of the loop between Ile13 Ca-Ser17
736 Ca is shown in a dotted line. **(C)** Electron density and atomic model of Glycine loop in FimH-DSG
737 TM. **(D)** Superimposition of FimH-DSG TM (orange), WT FimH in apo (PDB code 3JWN, light
738 grey) and trimannose-bound (PDB code 6GTV, slate) forms shows that the ligand binding site of
739 FimH-DSG TM adopts an open conformation resembling the apo state but not the ligand-bound,
740 closed conformation.

741

742

743 **Fig. 6 Identification of novel inhibitory epitopes on FimH-DSG TM**

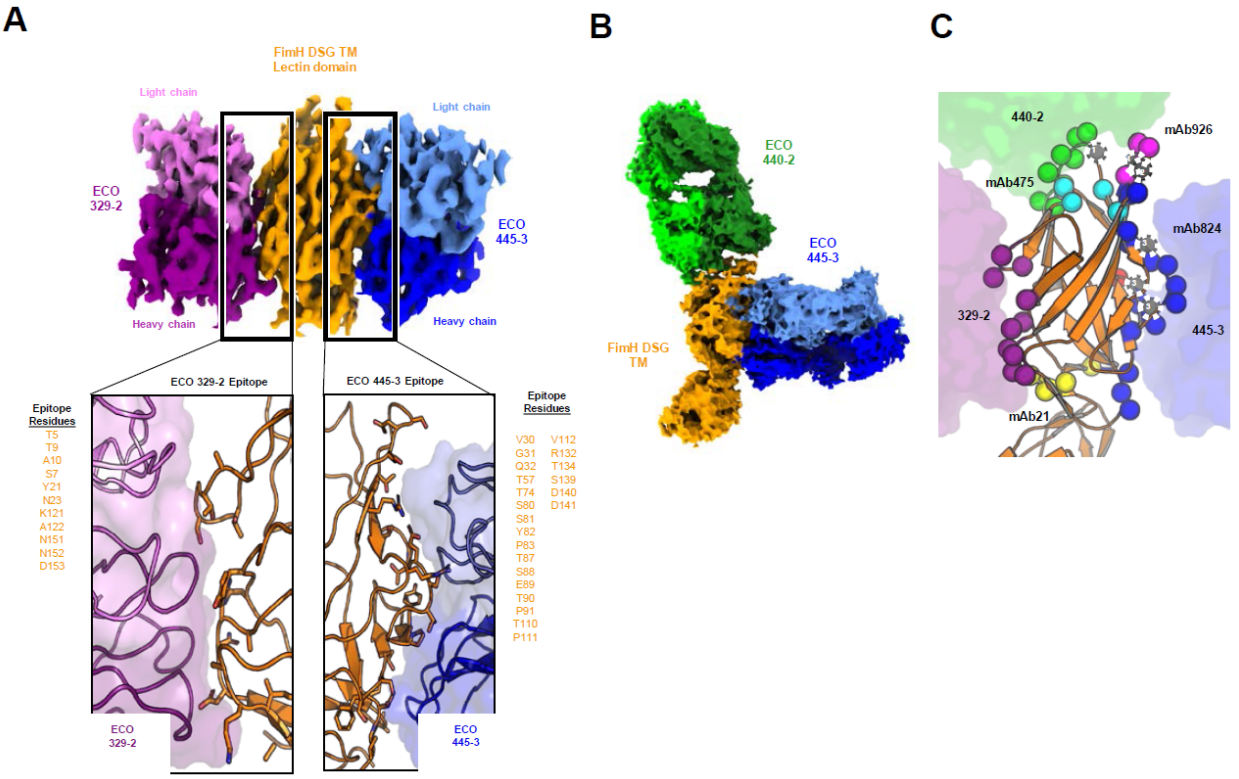

744

745 **(A)** Structure of FimH-DSG TM in complex with 329-2 and 445-3 Fabs solved by cryo-EM. Top
746 image shows the cryo-EM map, colored by chain, as indicated. Insets show respective epitope
747 interfaces, with FimH residues contributing to each epitope surface shown in stick representation
748 and listed along the side. **(B)** CryoEM structure of FimH-DSG TM in complex with 440-2 and
749 445-3 Fabs, colored by chain, as indicated. While this map was not suitable for modeling, the Fabs
750 and respective epitopes could be distinguished by comparison to the structure in panel A. **(C)**
751 Cartoon representation of the $FimH_{LD}$ in the FimH-DSG TM crystal structure. Epitopes identified
752 in this study and in previous work by others (Mab 926, 824, 475 and 21) are highlighted, with
753 participating residues shown as spheres and colored as indicated. Numbered gray residues indicate
754 coincidence between two epitopes (1 = Mab 926 and Mab 475, 2 = Mab 926 and Mab 445-3, 3 =
755 Mab 475 and Mab 824).

756

Fig. 7 Structural basis of inhibitory mechanisms of different Mabs

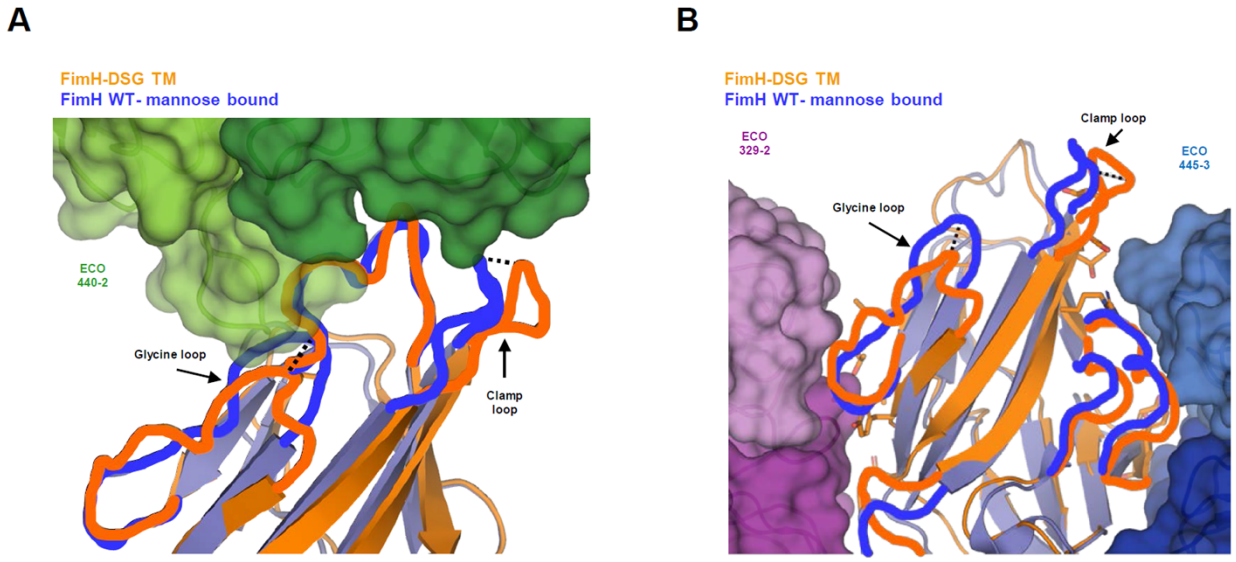

(A) Superimposition of FimH WT bound to trimannose (PDB code 6GTV, blue) and FimH-DSG TM (orange) cryo-EM structure resolved from the complex with Fabs of 440-2 (green surface) and 445-3 (not shown). **(B)** Superimposition of FimH WT bound to trimannose (PDB code 6GTV, blue) and FimH-DSG TM (orange) cryo-EM structure resolved from the complex with Fabs of 329-2 (purple) and 445-3 (dark blue). Surface representations for the two Fabs are shown. Side chains from FimH-DSG TM that are part of the Mab epitopes are shown in stick format. In **(A)** and **(B)**, shift of the clamp loop and Glycine loop from FimH-DSG TM to mannose-bound FimH WT is highlighted by dashed lines. Conformations of the important FimH epitope loops for 440-2, 329-2, and 440-2 binding are highlighted by orange (FimH-DSG TM structure) and blue (FimH WT-mannose bound structure) lines.

Table 1 Identification of novel FimH inhibitory antibodies

			Inhibitory (IC_{50}) titer, µg/ml	Kinetic Measurements with FimH-DSG WT (Averages with Stdev)						
Site	**Mab type**	**FimH Mabs**		**k_a (1/Ms)**	**k_a (1/Ms) Stdev**	**k_{dis} (1/s)**	**k_{dis} (1/s) Stdev**	**K_D (nM)**	**n**	**Elicited antigen**
1	Reference	475	26.4	1.9E+05	±2.6E4	5.7E-04	1.8E-04	3.1	8	
		926	0.4	1.9E+05	±5.3E4	6.5E-04	4.8E-05	0.9	5	
1	Ligand Binding epitope	299-3	1.4	4.1E+05	±2.5E4	3.4E-04	3.3E-05	0.8	4	FimH-DSG WT
		304-1	0.3	4.1E+05	±4.3E4	1.0E-04	1.6E-05	0.2	7	
		306-2	4.9	4.1E+05	±3.0E4	4.8E-04	1.5E-05	0.6	5	
		313-1	11.9	4.1E+05	±2.3E4	5.3E-04	1.2E-05	2.1	5	
		330-2	14.3	4.1E+05	±8.1E4	1.1E-03	1.6E-05	1.9	5	
		338-4	2.5	4.1E+05	±9.7E3	2.1E-04	1.4E-05	1.4	5	
2	Non-ligand binding site epitope	327-3	1.0	5.8E+05	±1.5E4	8.0E-05	6.3E-05	0.1	5	
		329-2	3.3	5.8E+05	±3.5E4	6.7E-05	1.8E-05	0.1	5	
3	Non-ligand binding site epitope	445-3	1.3	5.8E+05	±4.2E4	7.5E-05	2.8E-05	0.1	5	FimH DSG-LM
4	Non-ligand binding site epitope	440-2	94.8	9.4E+04	±1.9E4	6.2E-04	8.2E-05	7.0	5	

Mabs against FimH were screened for ability to inhibit bacterial binding in the bacterial inhibition assay. Resulting Mabs were subjected to a series of competition experiments to identify groups of antibodies likely binding similar epitopes. This table shows inhibitory titers of each antibody and relative FimH binding affinity. Two Mabs, 440-2 and 445-3, were derived from mice immunized with a conformationally locked version of FimH, FimH-DSG LM (V27C L34C).

Supplementary Materials

1. Supplementary Methods

1.1. X-ray crystallography of FimH-DSG TM

For X-ray crystallography experiments, FimH-DSG TM was expressed in ExpiCHO cells (Thermo Fisher Scientific) as secreted proteins with C-terminal His tags. Cell culture supernatant was harvested and 1 M Tris pH 7.4 and 5 M NaCl were added to final concentrations of 20 mM and 150 mM final concentrations respectively. A 5 kDa TFF cassette buffer was rinsed and equilibrated in 20 mM Tris pH 7.5 with 500 mM NaCl and 40 mM imidazole. Supernatant was concentrated 2-fold and diafiltered against 6 volumes of 20 mM Tris pH 7.5 500 mM NaCl 40 mM imidazole. Retentate was collected and filtered with a 0.2 um bottletop filter. An XK26/20 column was packed with Ni-Sepharose 6 Fast Flow resin (Cytiva Life Sciences) and equilibrated with 5 column volumes of 20 mM Tris pH 7.5 500 mM NaCl 40 mM imidazole. Retentate was applied at half flow rate and washed until a stable baseline was reached (approximately 55 column volumes). Bound protein was eluted with 20 mM Tris, 500 mM NaCl, 500 mM imidazole, pH 7.5. Fractions containing the protein of interest were pooled and dialyzed in a 2 kDa dialysis cassette against 20 mM sodium acetate, pH 4.3 at 4 ºC with two buffer changes. Protein was applied to a SP-Sepharose cation exchange column (Cytiva Life Sciences) that had been equilibrated with the same buffer. Material bound to the cation-exchange resin was eluted with a linear gradient of NaCl using 20 mM sodium acetate, pH 4.3, 1 M NaCl buffer. Fractions were pooled, and dialyzed against TBS, pH 7.4.

Purified FimH-DSG TM was buffer exchanged against 20 mM Tris (pH 7.5) using PD-10 column and concentrated to 10 mg/ml. Crystallization was performed at 20 °C using sitting drop vapor diffusion method by mixing equal volumes of protein and reservoir solution containing 1 M sodium acetate (pH 4.5) and 25% (w/v) PEG3350. Crystals grew to their maximum size in ~ 7 days. Crystals were cryoprotected using the reservoir solution supplemented with 15% glycerol and flash frozen in liquid nitrogen. Diffraction data were collected at APS 17-ID. The data was processed using autoPROC (Global Phasing Limited) and

the structure was solved using WT FimH-DSG complex (PDB code 4XOD) as a starting model (18). Model building and refinement were carried out using COOT and BUSTER (Global Phasing Limited).

1.2. Binning of monoclonal antibodies

Of the 300 parents Mabs screened in the *E. coli* binding inhibition assay, 34 parents were inhibitory; hybridomas from these parents were expanded and 26/34 survived the expansion. From these, 30 ml supernatant was purified using protein A/G resin on gravity flow columns. 12 of the 26 parents had inhibitory activity, evaluated in a 7-point titration assay starting at 75 nM with 2-fold serial dilutions. These hybridomas were cloned, and 3 clones of each were screened again for neutralizing activity. This led to the selection of independent 10 Mab clones with neutralizing activity (**Table 1**).

Epitope binning and kinetics experiments were performed on an Octet HTX instrument. For each epitope binning experiment, Ni-NTA Biosensors (Sartorius Cat# 18-5103) were pre-wet in assay buffer containing 1x PBS 1% BSA 0.1 % tween 20 for at least 10 minutes. To establish the initial baseline, Ni-NTA biosensors were immersed in assay buffer for 60 sec. His-tagged mammalian $FimH_{LD}$ WT ($mFimH_{LD}$ WT) was loaded at 5 ug/ml for 300 sec onto the baseline-established biosensors. $mFimH_{LD}$ WT-loaded and baseline established biosensors were allowed to bind first Mab at 5 ug/ml for 5 min. the baseline was re-established in assay buffer for 3 min. Finally, the first Mab-loaded and baseline-established biosensors were allowed to bind competing Mab (5 µg / ml) for 300 seconds. The nm shift response was measured for all the antibodies under investigation. Antibodies competing against each other should have low binding response whereas the Mabs binding to different epitopes results in higher binding.

To measure kinetic measurements of different FimH Mabs, anti-mouse IgG Fc (AMC Biosensors, cat# 18-5090) were pre-wet in assay buffer for at least 10 min. The initial baseline was established with pre-wet AMC biosensors in assay buffer for 60 seconds. FimH monoclonal antibodies at 1 µg/ml were loaded onto baseline-established biosensors until the nm threshold reached 1 nm, or for 600 seconds. The baseline was re-established for Mab-loaded biosensors in assay buffer, for 3 minutes. Mab-loaded and

baseline-established biosensors were allowed to bind 2-fold dilutions of mammalian derived $FimH_{LD}$ WT (starting at 100 nM), for 300 seconds followed by dissociation for 25 min. Results were processed in Data Evaluation v11.1 HT, by subtracting the sensorgram of 0 nM mammalian WT $FimH_{LD}$ blank from the rest of the dilutions. All sensorgrams were aligned to the baseline step followed by aligning the dissociation and association steps. Curves were fit with a Langmuir 1:1 global fit to obtain kinetic measurements. Average values obtained from 2 to 3 experiments were tabulated.

1.3. Sample Preparation for FimH-DSG Fab complex Cryo-EM

To prepare FimH DSG complex with Fabs for analysis by cryo-EM, FimH DSG was combined with a 1.25-fold molar excess each of ECO-329-2 Fab and ECO-445-3 Fab and incubated for 2 hours on ice. The mixture was fractionated by size-exclusion chromatography on a Superdex 200 5/150 GL gel filtration column pre-equilibrated in 20 mM HEPES pH 7.5, 150 mM NaCl. Fractions corresponding to the ternary complex were pooled and concentrated to 0.25 mg/ml in a 3 kDa NMWCO Amicon centrifugal ultrafiltration concentrator. This sample was used for grid vitrification for cryo-EM.

Prior to vitrification, 0.3% β-octylglucoside was added to the sample. The sample was then subjected to centrifugation at 13,200 x *g* for 10 min to remove large aggregates. Gold Quantifoil R1.2/1.3 200 mesh grids were made hydrophilic by glow discharge in residual air at 15 mA for 30 seconds using a Pelco Easiglow. Grids were vitrified using a Vitrobot Mark IV at 4°C and 100% humidity. 4 µl of the sample supernatant was applied to Quantifoil Au 200 mesh R1.2/1.3 grids glow discharged in residual air, then blotted from both sides before plunge-freezing in liquid ethane. Grids were stored under liquid nitrogen until imaging.

1.4. Cryo-EM Data Collection and Processing

Grids were imaged in a Titan Krios G2 transmission electron microscope operated at 300 kV equipped with a Falcon 4i direct electron detector and Selectris X imaging filter. All screening and data collection were performed in EPU (Thermo Fisher Scientific). Movies in EER format were collected at 215,000x

magnification (0.59 Å magnified pixel size at the specimen level) with a total electron dose of 50 e^-/ Å^2. A dataset of 7,584 movies was collected. Movies were subjected to patch motion correction (nominal pixel size = 0.59 Å, EER fractionation into 40 frames, without upsampling) and patch CTF correction in CryoSPARC 3.3.1. Manual particle picking was used to pick 348 particles, which were subjected to 2D classification to yield templates for template-based particle autopicking. Template-based autopicking against the full dataset yielded 861,802 particles, which were extracted in 500-pixel (29.5 nm) boxes Fourier-cropped to 250 pixels (1.18 Å/pixel) and subjected to multiple rounds of 2D classification to remove damaged particles or non-particle picks from the dataset. 199,906 particles were subjected to ab initio modeling in 4 classes. The most well-defined model, comprising 80,368 particles, was subjected to non-uniform 3D gold-standard refinement and reached a resolution of 3.11 Å, but the model quality was compromised by flexibility in the Fc portions of the Fabs and the FimH pilin domain. To improve the model quality, these portions of the map were subtracted using particle subtraction in CryoSPARC, and the subtracted particles were subjected to 3D gold-standard local refinement against the model, using the pose/shift gaussian prior during alignment and cross-validation-optimal non-uniform regularization. The resulting model was resolved to 3.12 Å with significantly improved model quality.

1.5. Model Building and Refinement

To model each of the components, atomic coordinates from the FimH DSG crystal structure reported here and from PDB entries 4U0R, 7C61, 6H3H, and 7DNH for the Fabs (based on their sequence homology to the heavy and light chains of Fabs 329-2 and 445-3, respectively) were rigid-body fitted into the cryo-EM map density. Sequence modifications were made to each of the models to match those of the molecules used in the experiment, then the model was successively hand-built into the map using Coot v0.9.8.1 in alternation with real-space refinement in Phenix v1.20 to produce the final model. The full cryo-EM data processing workflow and validation metrics can be found in the supplementary materials. Figures based on the structure were produced in PyMol v2.5.4, UCSF Chimera v1.16, and ChimeraX v1.4.

2. Supplementary data tables

Table S1 Bacterial binding inhibitory titers induced by E. coli and mammalian produced FimH proteins in mice

Group	Responder rate (%)	# of responders (N=20)	Binding inhibition /geometric mean IC_{50}
Periplasmic $FimH_{LD}$ WT	55	11	300
Periplasmic $FimH_{LD}$ V27C L34C	40	8	254
Mammalian $FimH_{LD}$ WT	45	9	194
Mammalian $FimH_{LD}$ V27C L34C	10	2	73
Mammalian FimH-DSG WT	75	15	529
Mammalian FimH-DSG V27C L34C	80	16	579
Periplasmic FimCH	67	12 (N=18)	354

881 **Table S3 Binding K_d of FimH mutants to octylbiphenylmannopyranoside ligand**

Design category	FimH variant	Replicates	Average K_d / nM
WT	$FimH_{LD}$ WT	12	0.2±0.0
	$FimH_{LD}$ V27A	3	0.2±0.0
Reference mutations	$FimH_{LD}$ R60P	1	4.5
	$FimH_{LD}$ V27A R60P	6	34.6±8.2
	$FimH_{LD}$ V27C L34C	7	17.7±3.1
Glycine switch mutations in the $FimH_{LD}$	$FimH_{LD}$ G15P	1	>2000
	$FimH_{LD}$ G15P V27A	4	>2000
	$FimH_{LD}$ G15A	1	46.7
	$FimH_{LD}$ G15A V27A	4	>2000
	$FimH_{LD}$ G16P	1	>2000
	$FimH_{LD}$ G16P V27A	4	>2000
	$FimH_{LD}$ G16A	1	9.6
	$FimH_{LD}$ G16A V27A	3	30.2±0.8
Glycine switch mutations in the $FimH_{LD}$	$FimH_{LD}$ G15A G16A V27A	4	>2000
	$FimH_{LD}$ V27A G65A	1	4.6
Cysteine pairs for disulfide bond stabilization in the $FimH_{LD}$	$FimH_{LD}$ V28C N33C	2	6.5±2.1
	$FimH_{LD}$ V28C P157C	1	7.7
	$FimH_{LD}$ P26C V154C	1	8.4
Nonpolar-to-polar mutations in $FimH_{LD}$	$FimH_{LD}$ L34T V27A	1	0.4
	$FimH_{LD}$ L34N V27A	1	1.7
	$FimH_{LD}$ A119T V27A	1	0.4
	$FimH_{LD}$ A119N V27A	1	1

Substitutions in the ligand binding site of $FimH_{LD}$	$FimH_{LD}$ F1Y	2	0.3
	$FimH_{LD}$ F1W	1	48.4
	$FimH_{LD}$ F1M	1	>2000
	$FimH_{LD}$ F1L	1	534
	$FimH_{LD}$ F1I	1	>2000
	$FimH_{LD}$ F1V	1	472
Full length WT FimH	FimH-DSG WT	12	23.4±7.6
	FimH-DSG V27A	2	53.6±9
Cysteine pairs for disulfide bond stabilization in the $FimH_{LD}$, in full length FimH	FimH-DSG V27C L34C	3	59.9±28.2
Glycine switch mutations in the $FimH_{LD}$, in full length FimH	FimH-DSG G15A V27A	2	>2000
	FimH-DSG G16A V27A	2	>2000
	FimH-DSG G15A G16A V27A	6	>2000
Cavity-filling mutations at the Pilin-Lectin interface of FimH-DSG	FimH-DSG A115I	1	9.8
	FimH-DSG V185I	1	21

882

883

884 **Table S4 Melting temperature of FimH mutants in apo state and in the presence of methyl alpha-D-**

885 **mannopyranoside**

Design category	FimH variant	Replicates	Tm (Average) / ºC	ΔTm (Average) / ºC
WT	$FimH_{LD}$ WT	11	61.5±0.8	11.0±0.8
	$FimH_{LD}$ V27A	6	59.9±0.9	10.0±0.6
Reference	$FimH_{LD}$ R60P	2	56.3±0.2	8.4±1.7
	$FimH_{LD}$ V27A R60P	3	60.1±0.4	3.1±0.5
Glycine switch mutations in the $FimH_{LD}$	$FimH_{LD}$ G15A	3	56.3±0.1	3.8±0.4
	$FimH_{LD}$ G15P	2	56.0±1.1	2.9±0.1
	$FimH_{LD}$ G16A	2	54.6±0.3	6.1±0.3
	$FimH_{LD}$ G16P	2	55.3±0.6	1.5±0.3
	$FimH_{LD}$ G15A V27A	4	57.8±0.5	1.5±0.5
	$FimH_{LD}$ G15P V27A	2	58.2±0.6	1.3±0.6
	$FimH_{LD}$ G16A V27A	6	57.7±0.5	1.8±1.0
	$FimH_{LD}$ G16P V27A	5	58.2±0.5	0.8±0.8
	$FimH_{LD}$ G15A G16A V27A	3	59.1±0.4	0.4±0.5
Cysteine pairs for disulfide bond stabilization in the $FimH_{LD}$	$FimH_{LD}$ V28C N33C	5	65.8±1.1	2.8±0.2
	$FimH_{LD}$ V27C L34C	7	51.4±0.8	7.3±0.6
	$FimH_{LD}$ P26C V154C	4	60.4±1.8	5.7±1.1
	$FimH_{LD}$ P26C V156C	1	58.9	5.4
	$FimH_{LD}$ Q32C Y108C	1	61.1	9.8
	$FimH_{LD}$ P26C V154C	1	62.5	4.7
	$FimH_{LD}$ V28C P157C	1	59.6	7.2
	$FimH_{LD}$ S62C T86C	1	58.3	11.7

	$FimH_{LD}$ S62C L129C	1	57.1	12.8
	$FimH_{LD}$ Y64C A127C	1	60.2	12.9
	$FimH_{LD}$ V112C T158C	1	59.6	15.2
	$FimH_{LD}$ V118C V156C	1	56.7	12.9
	$FimH_{LD}$ P12C A18C	1	54.5	5.2
	$FimH_{LD}$ G14C F144C	1	49.2	-0.1
	$FimH_{LD}$ L68C F71C	1	49.9	12.2
	$FimH_{LD}$ S113C G116C	1	59.8	9.3
	$FimH_{LD}$ A119C V155C	1	59.1	14.5
Substitutions in the ligand binding site of $FimH_{LD}$	$FimH_{LD}$ F1I	2	55.2±0.0	0.3±1.2
	$FimH_{LD}$ F1L	2	60.1±0.2	0.8±0.5
	$FimH_{LD}$ F1M	3	52.7±1.5	1.1±1.6
	$FimH_{LD}$ F1V	3	52.4±0.1	0.7±0.9
	$FimH_{LD}$ F1W	3	52.8±0.6	4.5±0.6
	$FimH_{LD}$ F1Y	3	54.2±0.2	10.1±0.3
Nonpolar-to-polar mutations in $FimH_{LD}$	$FimH_{LD}$ L34S V27A	1	48.9	12.8
	$FimH_{LD}$ L34T V27A	1	53.2	10.5
	$FimH_{LD}$ L34N V27A	1	47.3	13.1
	$FimH_{LD}$ A119S V27A	1	59.8	8.5
	$FimH_{LD}$ A119T V27A	1	59.5	9.2
	$FimH_{LD}$ A119N V27A	1	57.9	7.6
	$FimH_{LD}$ V27A G65A	1	59.8	10.9
Full length WT FimH	FimH-DSG WT	11	71.7±0.5	2.1±0.2

Cysteine pairs for disulfide bond stabilization in the $FimH_{LD}$, in full length FimH	FimH-DSG V27C L34C	6	63.3±1.2	1.3±0.5
Full length WT FimH	FimH-DSG V27A	5	72.6±0.6	-0.4±0.2
Glycine switch mutations in the $FimH_{LD}$, in full length FimH	FimH-DSG G15A V27A	5	73.0±0.6	-0.1±0.3
	FimH-DSG G16A V27A	5	72.3±0.5	-0.0±0.1
	FimH-DSG G15A G16A V27A	10	73.4±0.5	0.0±0.1
Cavity-filling mutations at the Pilin-Lectin interface of FimH-DSG	FimH-DSG A115I	2	68.5±0	4.1
	FimH-DSG V185I	2	71.4±0.5	2.5±0.4
	FimH-DSG DSG V3I	1	70.7	3.1
	FimH-DSG V163I	1	70.4	3.5
Ligand binding blocking mutation in $FimH_{LD}$, in full length FimH	FimH-DSG Q133K	1	71.6	1.7
Ligand binding blocking mutation in	FimH-DSG V27A Q133K	1	75.1	0.1

$FimH_{LD}$, in full length FimH				
Ligand binding blocking mutation in $FimH_{LD}$ combined with glycine loop mutations, in full length FimH	FimH-DSG G15A G16A V27A Q133K	1	73.9	1.3

886

887

888 **Table S5 Mab binding to $FimH_{LD}$ mutants**

FimH variant	Response (nm)		
	Monoclonal antibody		
	299-3	304-1	440-2
$FimH_{LD}$ WT	3.10	3.02	0.04
$FimH_{LD}$ V27A	0.44	0.54	0.06
$FimH_{LD}$ V27A R60P	3.19	3.03	0.85
$FimH_{LD}$ V27A G15A	3.31	3.03	0.78
$FimH_{LD}$ V27A G15P	3.07	2.95	0.62
$FimH_{LD}$ V27A G16A	3.44	3.20	0.75
$FimH_{LD}$ V27A G16P	3.26	3.16	0.88
$FimH_{LD}$ G15A G16A V27A	3.34	3.06	0.79
$FimH_{LD}$ V27C L34C	3.11	2.77	0.81
$FimH_{LD}$ V28C N33C	3.054	2.74	0.72
$FimH_{LD}$ P26C V154C	3.11	2.89	0.83

889

890

891 **Table S6 Mab binding to FimH-DSG variants**

FimH variant	**Response (nm)**		
	Monoclonal antibody		
	299-3	**304-1**	**440-2**
FimH-DSG WT	2.44	2.22	0.38
FimH-DSG V27A	2.48	2.17	0.35
FimH-DSG V27C L34C	2.35	2.23	0.33
FimH-DSG V27A G15A	2.52	2.30	0.37
FimH-DSG V27A G16A	2.69	2.42	0.42
FimH-DSG G15A G16A V27A	2.68	2.30	0.49

892

893

894 **Table S7 Bacterial binding inhibitory titers induced by $FimH_{LD}$ and FimH-DSG mutants proteins in**

895 **mice**

Protein	IC_{50} GMTs		Responder rate (%)		Responders (n)		Mice (n)	
	PD2	PD3	PD2	PD3	PD2	PD3	PD2	PD3
$FimH_{LD}$ WT	89	191	20	40	4	8	20	20
$FimH_{LD}$ V27A	104	439	26	61	5	11	19	18
FimH-DSG V27A	1175	6102	78	100	14	18	18	18
$FimH_{LD}$ G15A V27A	57	683	5	53	1	10	20	19
FimH-DSG G15A V27A	1740	3400	84	100	16	19	19	19
$FimH_{LD}$ G15P V27A	58	346	5	42	1	8	20	19
$FimH_{LD}$ G16A V27A	93	1193	13	69	2	11	16	16
$FimH_{LD}$ G16P V27A	91	352	10	45	2	9	20	20
$FimH_{LD}$ G15A G16A V27A	111	1307	26	63	5	12	19	19
FimH-DSG G15A G16A V27A	1869	2386	84	95	16	18	19	19
$FimH_{LD}$ V27A R60P	212	1056	32	63	6	12	19	19
$FimH_{LD}$ V28C N33C	103	461	16	53	3	10	19	19

896

897

898 **Table S8 Neutralizing epitopes are preserved in four aglycosylated variants of the FimH DsG triple**

899 **mutant antigen**

	Response (nm)				
	Aglycosylated FimH-DSG TM variants				**Glycosylated FimH-DSG TM**
mAb	N228S N235S	T230A T237A	N228G N235G	N228Q N235Q	N235
299-3	0.22	0.23	0.22	0.22	0.25
306-2	0.24	0.26	0.25	0.26	0.27
926	0.49	0.47	0.48	0.49	0.55
329-2	0.24	0.23	0.25	0.24	0.27
440-2	0.13	0.11	0.11	0.13	0.17
445-3	0.27	0.28	0.31	0.27	0.30

900

901

902

903

904

905

906

907

908

909

910

911 **Table S9 X-ray data collection and refinement statistics for FimH DSG**

	FimH DSG (pdb code: 8V3J)
Data collection	
Space group	C121
Cell dimensions	
a, *b*, *c* (Å)	140.04, 149.26, 99.35
α, β, g (°)	90.00, 130.03, 90.00
Resolution (Å)	87.09-1.90 (2.04-1.90)*
R_{sym} or R_{merge}	0.05 (0.64)
I / sI	13.5 (1.33)
Completeness (%)	70.4 (49.2)
Redundancy	3.3 (2.3)
Refinement	
Resolution (Å)	87.09-1.90
No. reflections	86513
R_{work} / R_{free}	0.191 / 0.222
No. atoms	
Protein	8712
Water	1315
B-factors (Å^2)	
Mean, all atoms	50.0
R.m.s. deviations	
Bond lengths (Å)	0.008

Bond angles (°)	1.03
Ramachandran plot Favored (%)	99.0
Allowed (%)	1.0
Disallowed (%)	0

*Values in parentheses are for highest-resolution shell.

915 **Table S10 Cryo-EM data and refinement statistics**

Data collection and processing	**FimH DSG TM + Fab 440-2 + Fab 445-3**	**FimH DSG TM + Fab 329-2 + Fab 445-3 (EMDB-43048) (PDB 8V93)**
Magnification	165,000x	215,000x
Voltage (kV)	300	300
Electron exposure (e–/Å^2)	50	50
Defocus range (μm)	-3.2 to -1.2	-2.4 to -0.6
Pixel size (Å)	0.87	0.59
Symmetry imposed	C1	C1
Initial particle images (no.)	2,817,610	861,802
Final particle images (no.)	199,492	80,368
Map resolution (Å) FSC threshold	3.9 (0.143)	3.12 (0.143)
Refinement		
Initial model used (PDB code)		4U0R, 7C61, 6H3H, 7DNH
Model resolution (Å) FSC threshold		3.9 0.5
Map sharpening *B* factor (Å^2)		82.7
Model composition Non-hydrogen atoms		 4,677

Protein residues		613
Ligands		0
B factors (Å^2)		
Protein		29.58/100.90/56.49
Ligand		N/A
R.m.s. deviations		
Bond lengths (Å)		0.005
Bond angles (°)		0.969
Validation		
MolProbity score		1.826.54
Clashscore		0
Poor rotamers (%)		
Ramachandran plot		
Favored (%)		92.82
Allowed (%)		7.01
Disallowed (%)		0.17

916

917

918

919

3. Supplementary figures

Fig. S1 Optimization of full length FimH production in Expi293 cells

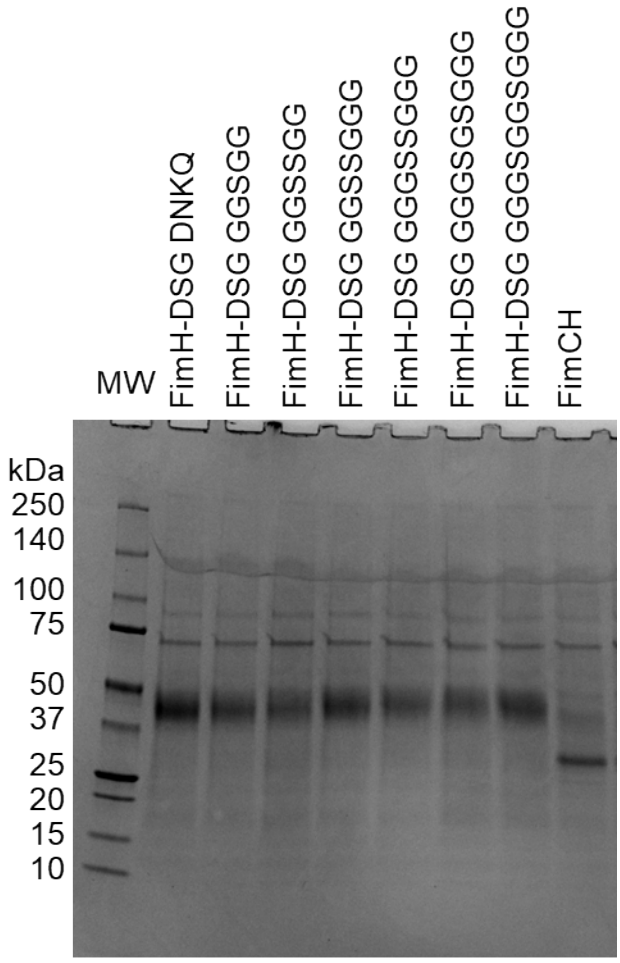

Expi293 cells were transfected with constructs encoding FimH-DSG with linkers (DNKQ, GGSSGG, etc.) and the FimCH complex. Raw culture supernatants collected 96 hours post transfection were loaded on an SDS-PAGE gel and stained with Coomassie blue.

928 **Fig. S2 Informative regions of CD spectra of $FimH_{LD}$ and FimH-DSG mutants**

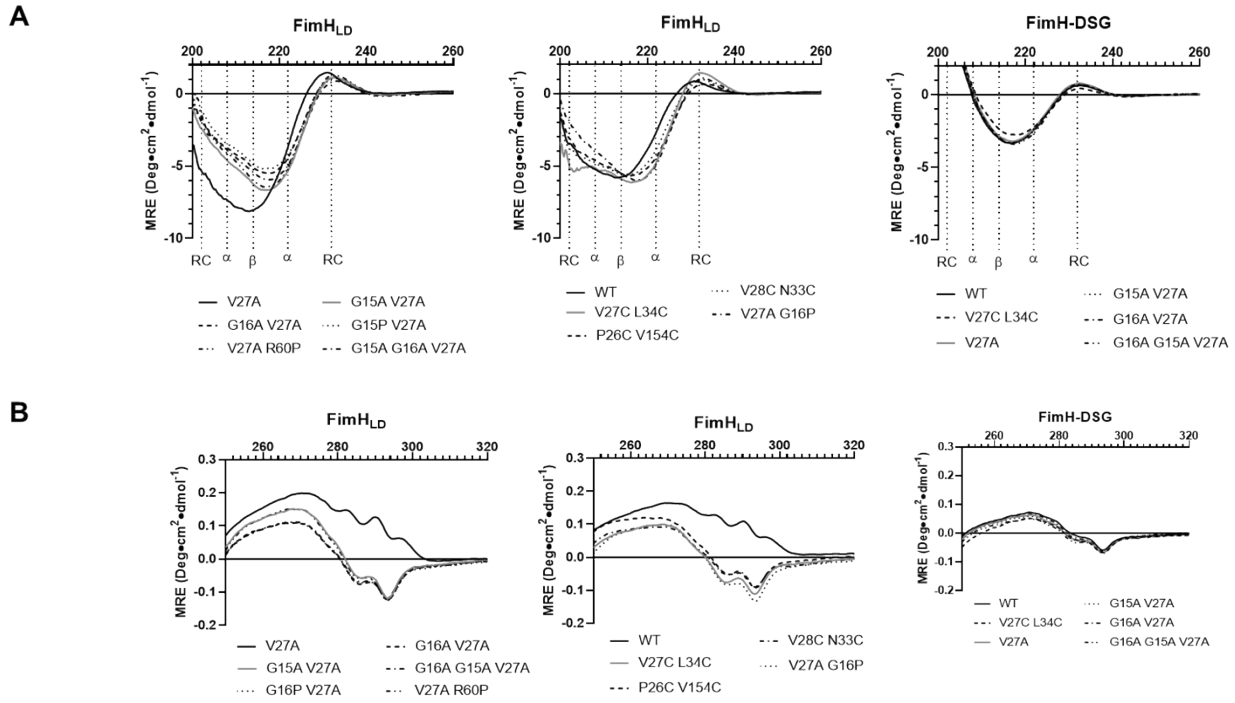

929

930

931 CD spectra in the far-UV **(A)**, reporting on the secondary structure, and near-UV **(B)**, reporting on the

932 tertiary structure of FimH variants.

933

Fig. S3 FimH-DSG TM can be purified to homogeneity from ExpiCHO supernatants

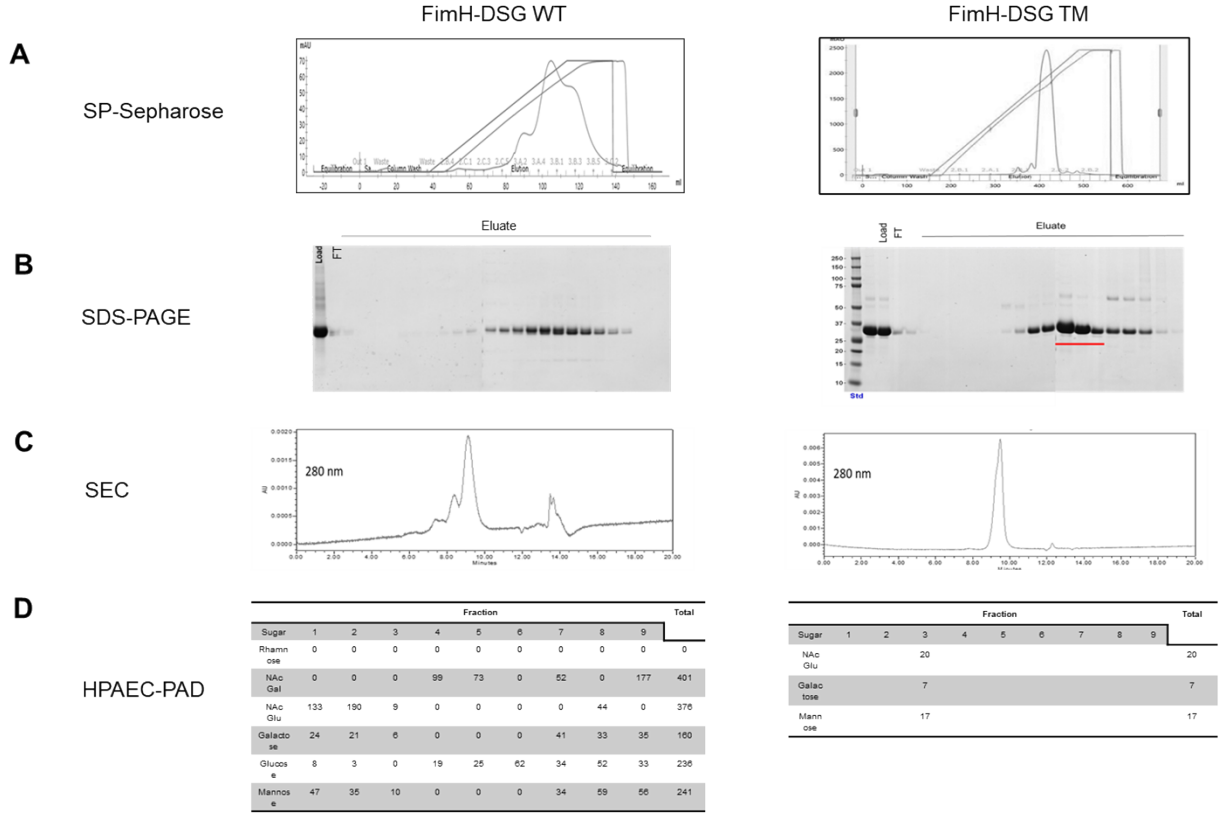

Fraction										Total
Sugar	1	2	3	4	5	6	7	8	9	
Rhamnose	0	0	0	0	0	0	0	0	0	0
NAc Gal	0	0	0	99	73	0	52	0	177	401
NAc Glu	133	190	9	0	0	0	0	44	0	376
Galactose	24	21	6	0	0	0	41	33	35	160
Glucose	8	3	0	19	25	62	34	52	33	236
Mannose	47	35	10	0	0	0	34	59	56	241

Fraction										Total
Sugar	1	2	3	4	5	6	7	8	9	
NAc Glu			20							20
Galactose			7							7
Mannose			17							17

To produce protein for structural characterization, FimH-DSG WT and FimH-DSG TM proteins were expressed in ExpiCHO cells as secreted proteins containing C-terminal His tags. (A) Elution profile of FimH-DSG WT (left panel) and FimH-DSG TM (right panel) on SP-Sepharose column. (B) SDS-PAGE analysis of eluted fractions. (C) Analytical SEC of FimH-DSG WT (left panel); wild type FimH-DSG TM (right panel). (D) Normalized amounts of monosaccharides (µg / mg protein) detected by HPAEC-PAD in various SP-Sepharose fractions from FimH-DSG WT and the main peak of FimH-DSG TM.

Fig S4 FimH-DSG aglycosylation variants have similar ability to elicit antibodies that inhibit bacterial binding compared to glycosylated parent

A

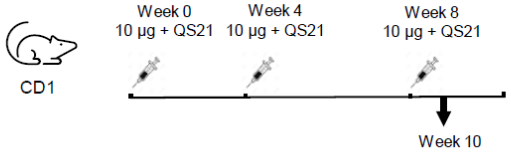

B

Group	Responder rate (%)	# of responders / N mice	Binding inhibition / geometric mean IC_{50}
FimH-DSG TM	89	16/18	525
FimH-DSG TM N235S	95	18/19	736
FimH-DSG TM N235Q	81	13/16	393

C

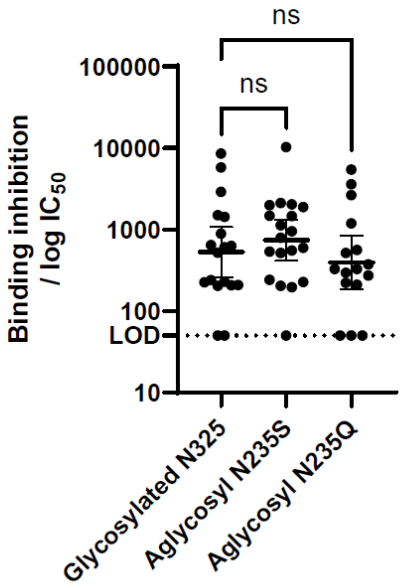

(A) Groups of 20 CD-1 mice (7-9 weeks old) were vaccinated subcutaneously with 0.1 mL of 10 mg of FimH-DSG antigens adjuvanted with 20 mg QS21/PS80 at weeks 0, 4 and 8. **(B)** Sera from week 6 and week 10 timepoints were tested for activity in the E. coli binding inhibition assay with geometric mean IC_{50} titers reported. Inhibitory titers were determined from serial dilution of sera from vaccinated mice and represent the reciprocal of the dilution of serum at which 50% of bacteria remain bound to the plate and are shown for post dose 3 timepoint. Statistical significance (p-value) of differences in responses between groups was determined using an unpaired t-test with Welch's correction applied to log-transformed data. Proportion of animals in each group responding to vaccine by exhibiting measurable IC_{50} titers are reported as % responder rates. **(C)** Figure displaying individual IC_{50} values; bars represent geometric mean and 95% confidence interval.

960 **Fig. S5 Visualization of linker region in structure of FimH-DSG TM**

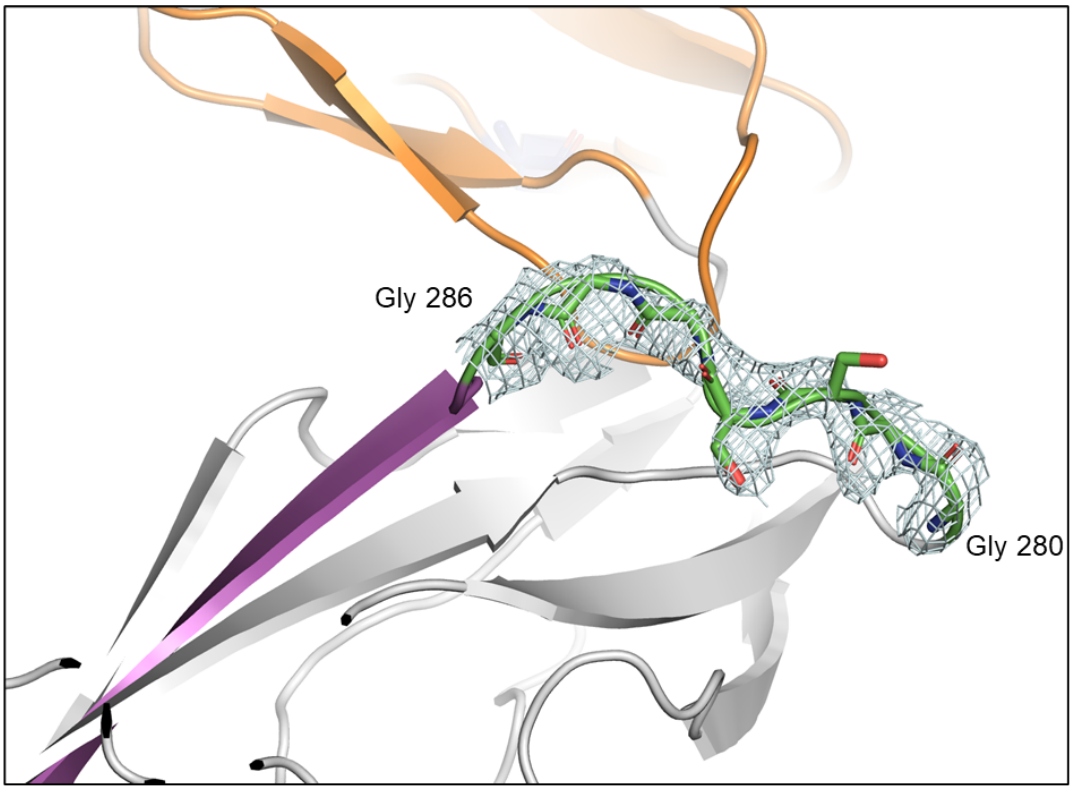

961

962 Electron density of the glycine-serine linker region. $FimH_{LD}$ is shown in orange, $FimH_{PD}$ is shown in grey,

963 the donor-strand peptide in pink and the glycine-serine linker in green.

964

965 **Fig. S6 Ability of Octylmannopyranoside to interfere with binding of monoclonal antibodies from**

966 **$FimH_{LD}$ WT**

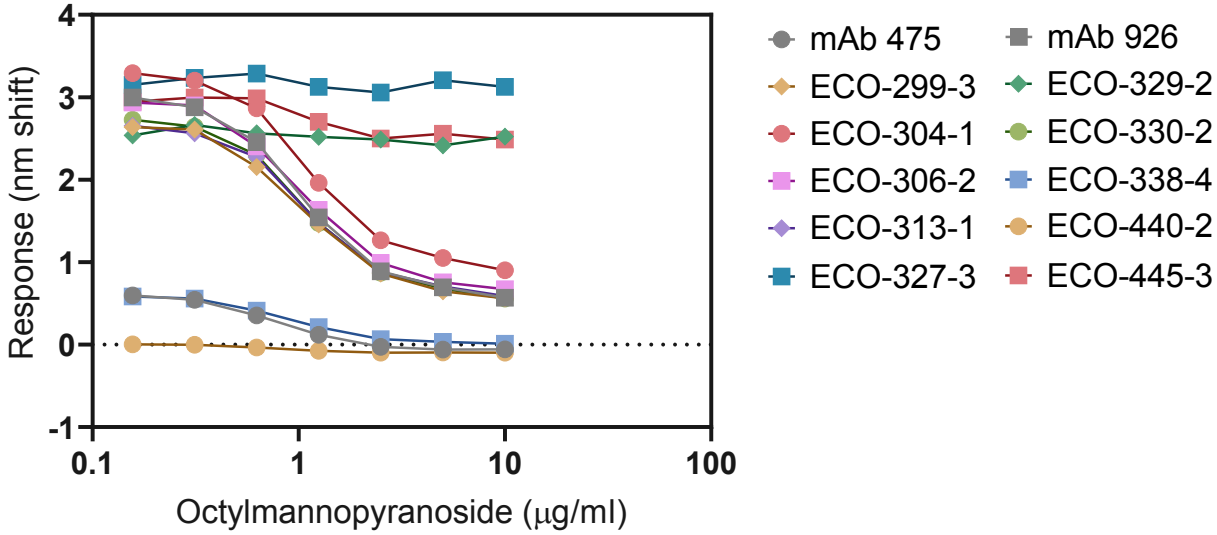

967

968 $FimH_{LD}$ WT was incubated with a two-fold dilution of Ocytlmannopyranoside ligand before loading onto

969 Octet Ni-NTA biosensors. FimH Mabs were allowed to bind at 5 μg/ml to the pre-bound $FimH_{LD}$ and

970 nanometer response measured for each dilution of the ligand.

971

972

973

974 **Fig. S7 Cryo-EM processing pipeline for FimH/329-2/445-3**

975

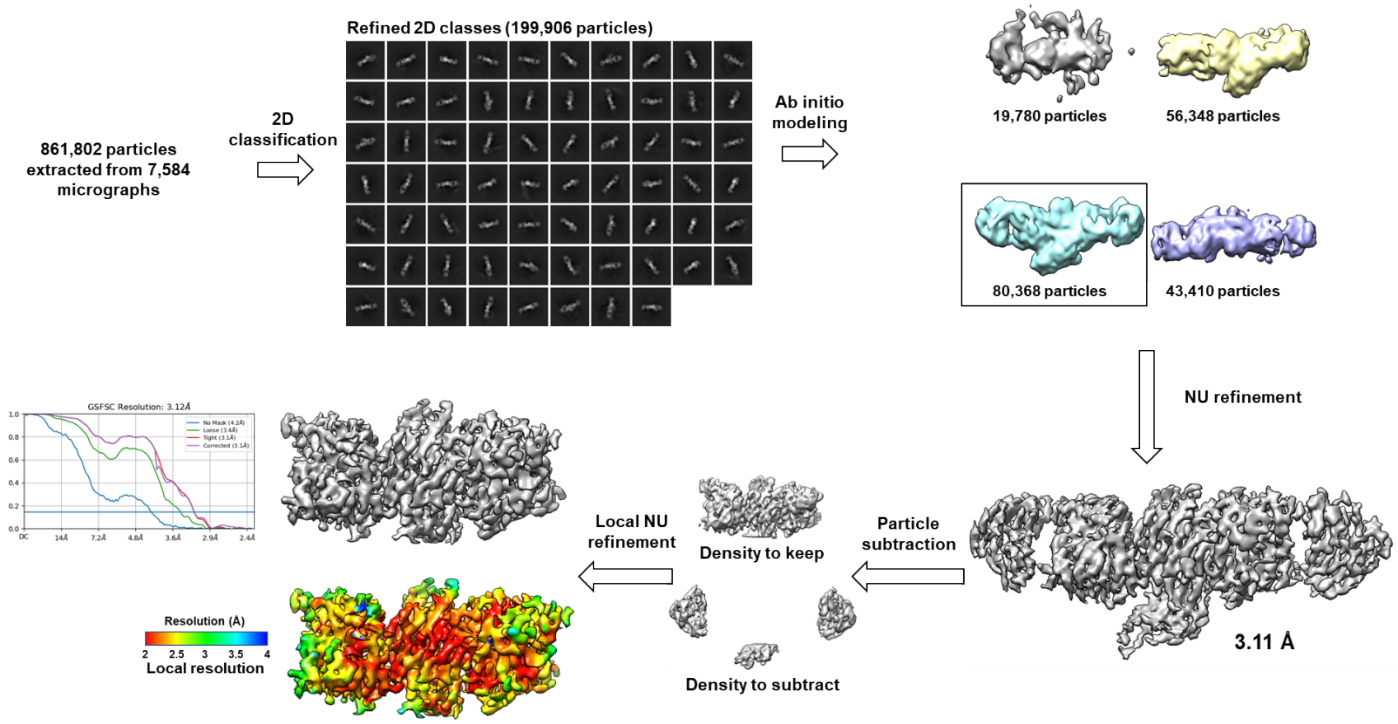

976

977

978 Cryo-EM data processing workflow in CryoSPARC for the FimH/329-2/445-3 ternary complex, with final

979 map colored by local resolution and Fourier shell correlation curves from gold-standard refinement.

980

981

982 **Fig. S8 Cryo-EM processing pipeline – FimH/440-2/445-3**

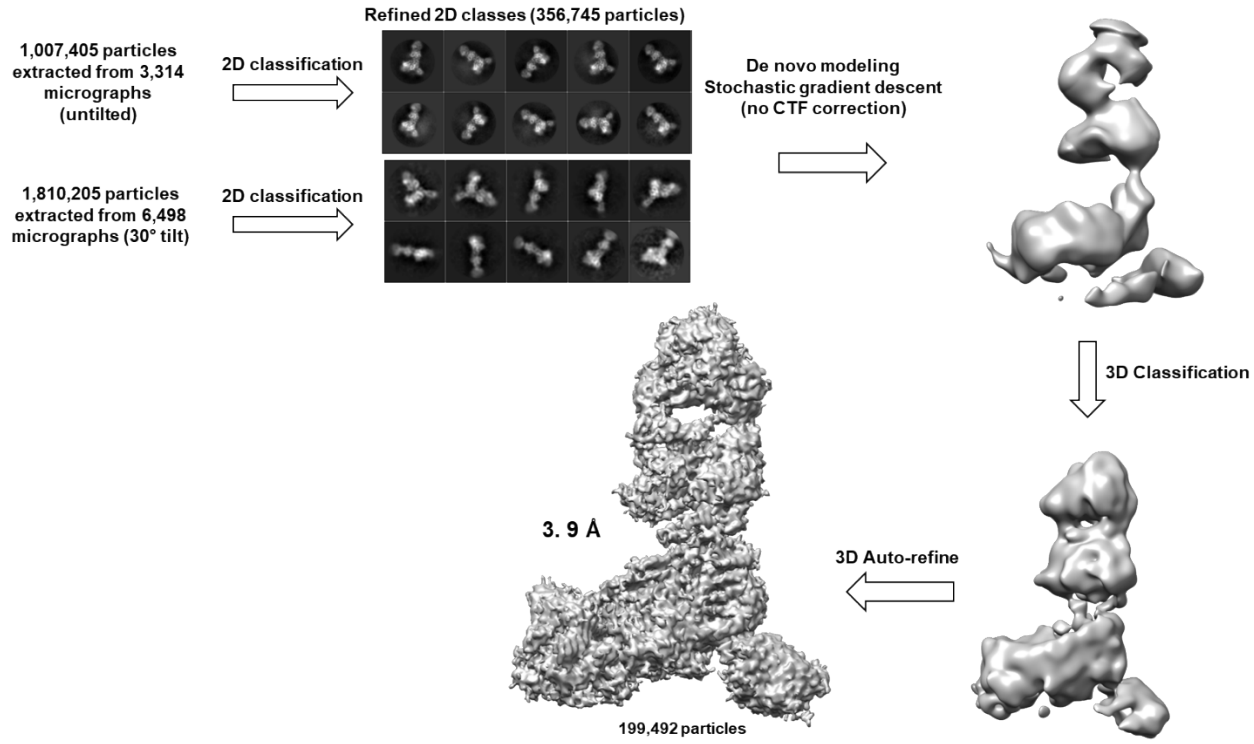

983

984

985 Cryo-EM data processing workflow in Relion for the FimH/440-2/445-3 ternary complex.

986

987

988

References

1. Foxman B. Urinary tract infection syndromes: occurrence, recurrence, bacteriology, risk factors, and disease burden. Infect Dis Clin North Am. 2014;28(1):1-13.
2. Zowawi HM, Harris PN, Roberts MJ, Tambyah PA, Schembri MA, Pezzani MD, et al. The emerging threat of multidrug-resistant Gram-negative bacteria in urology. Nat Rev Urol. 2015;12(10):570-84.
3. Flores-Mireles AL, Walker JN, Caparon M, Hultgren SJ. Urinary tract infections: epidemiology, mechanisms of infection and treatment options. Nature reviews Microbiology. 2015;13(5):269-84.
4. Terlizzi ME, Gribaudo G, Maffei ME. UroPathogenic Escherichia coli (UPEC) Infections: Virulence Factors, Bladder Responses, Antibiotic, and Non-antibiotic Antimicrobial Strategies. Front Microbiol. 2017;8:1566.
5. Wu XR, Sun TT, Medina JJ. In vitro binding of type 1-fimbriated Escherichia coli to uroplakins Ia and Ib: relation to urinary tract infections. Proc Natl Acad Sci U S A. 1996;93(18):9630-5.
6. Pak J, Pu Y, Zhang ZT, Hasty DL, Wu XR. Tamm-Horsfall protein binds to type 1 fimbriated Escherichia coli and prevents E. coli from binding to uroplakin Ia and Ib receptors. J Biol Chem. 2001;276(13):9924-30.
7. Jones CH, Pinkner JS, Roth R, Heuser J, Nicholes AV, Abraham SN, et al. FimH adhesin of type 1 pili is assembled into a fibrillar tip structure in the Enterobacteriaceae. Proc Natl Acad Sci U S A. 1995;92(6):2081-5.
8. Hannan TJ, Mysorekar IU, Hung CS, Isaacson-Schmid ML, Hultgren SJ. Early severe inflammatory responses to uropathogenic E. coli predispose to chronic and recurrent urinary tract infection. PLoS Pathog. 2010;6(8):e1001042.
9. Schwartz DJ, Chen SL, Hultgren SJ, Seed PC. Population dynamics and niche distribution of uropathogenic Escherichia coli during acute and chronic urinary tract infection. Infect Immun. 2011;79(10):4250-9.
10. Carey AJ, Tan CK, Ipe DS, Sullivan MJ, Cripps AW, Schembri MA, et al. Urinary tract infection of mice to model human disease: Practicalities, implications and limitations. Crit Rev Microbiol. 2016;42(5):780-99.
11. Schwartz DJ, Kalas V, Pinkner JS, Chen SL, Spaulding CN, Dodson KW, et al. Positively selected FimH residues enhance virulence during urinary tract infection by altering FimH conformation. Proc Natl Acad Sci U S A. 2013;110(39):15530-7.
12. Martinez JJ, Mulvey MA, Schilling JD, Pinkner JS, Hultgren SJ. Type 1 pilus-mediated bacterial invasion of bladder epithelial cells. EMBO J. 2000;19(12):2803-12.
13. Mulvey MA, Lopez-Boado YS, Wilson CL, Roth R, Parks WC, Heuser J, et al. Induction and evasion of host defenses by type 1-piliated uropathogenic Escherichia coli. Science. 1998;282(5393):1494-7.
14. Spaulding CN, Klein RD, Ruer S, Kau AL, Schreiber HL, Cusumano ZT, et al. Selective depletion of uropathogenic E. coli from the gut by a FimH antagonist. Nature. 2017;546(7659):528-32.
15. Mydock-McGrane L, Cusumano Z, Han Z, Binkley J, Kostakioti M, Hannan T, et al. Antivirulence C-Mannosides as Antibiotic-Sparing, Oral Therapeutics for Urinary Tract Infections. Journal of medicinal chemistry. 2016;59(20):9390-408.
16. Le Trong I, Aprikian P, Kidd BA, Thomas WE, Sokurenko EV, Stenkamp RE. Donor strand exchange and conformational changes during E. coli fimbrial formation. J Struct Biol. 2010;172(3):380-8.
17. Barnhart MM, Sauer FG, Pinkner JS, Hultgren SJ. Chaperone-subunit-usher interactions required for donor strand exchange during bacterial pilus assembly. J Bacteriol. 2003;185(9):2723-30.
18. Sauer MM, Jakob RP, Eras J, Baday S, Eris D, Navarra G, et al. Catch-bond mechanism of the bacterial adhesin FimH. Nat Commun. 2016;7:10738.

19. Rabbani S, Fiege B, Eris D, Silbermann M, Jakob RP, Navarra G, et al. Conformational switch of the bacterial adhesin FimH in the absence of the regulatory domain: Engineering a minimalistic allosteric system. J Biol Chem. 2018;293(5):1835-49.
20. Le Trong I, Aprikian P, Kidd BA, Forero-Shelton M, Tchesnokova V, Rajagopal P, et al. Structural basis for mechanical force regulation of the adhesin FimH via finger trap-like beta sheet twisting. Cell. 2010;141(4):645-55.
21. Aprikian P, Tchesnokova V, Kidd B, Yakovenko O, Yarov-Yarovoy V, Trinchina E, et al. Interdomain interaction in the FimH adhesin of Escherichia coli regulates the affinity to mannose. J Biol Chem. 2007;282(32):23437-46.
22. Nilsson LM, Thomas WE, Sokurenko EV, Vogel V. Elevated shear stress protects Escherichia coli cells adhering to surfaces via catch bonds from detachment by soluble inhibitors. Appl Environ Microbiol. 2006;72(4):3005-10.
23. Langermann S, Ballou WR, Jr. Vaccination utilizing the FimCH complex as a strategy to prevent Escherichia coli urinary tract infections. J Infect Dis. 2001;183 Suppl 1:S84-6.
24. Langermann S, Mollby R, Burlein JE, Palaszynski SR, Auguste CG, DeFusco A, et al. Vaccination with FimH adhesin protects cynomolgus monkeys from colonization and infection by uropathogenic Escherichia coli. J Infect Dis. 2000;181(2):774-8.
25. Langermann S, Palaszynski S, Barnhart M, Auguste G, Pinkner JS, Burlein J, et al. Prevention of mucosal Escherichia coli infection by FimH-adhesin-based systemic vaccination. Science. 1997;276(5312):607-11.
26. Habibi M, Asadi Karam MR, Shokrgozar MA, Oloomi M, Jafari A, Bouzari S. Intranasal immunization with fusion protein MrpH.FimH and MPL adjuvant confers protection against urinary tract infections caused by uropathogenic Escherichia coli and Proteus mirabilis. Mol Immunol. 2015;64(2):285-94.
27. Asadi Karam MR, Oloomi M, Mahdavi M, Habibi M, Bouzari S. Vaccination with recombinant FimH fused with flagellin enhances cellular and humoral immunity against urinary tract infection in mice. Vaccine. 2013;31(8):1210-6.
28. Wu J, Bao C, Reinhardt RL, Abraham SN. Local induction of bladder Th1 responses to combat urinary tract infections. Proc Natl Acad Sci U S A. 2021;118(10).
29. Thankavel K, Madison B, Ikeda T, Malaviya R, Shah AH, Arumugam PM, et al. Localization of a domain in the FimH adhesin of Escherichia coli type 1 fimbriae capable of receptor recognition and use of a domain-specific antibody to confer protection against experimental urinary tract infection. J Clin Invest. 1997;100(5):1123-36.
30. Brumbaugh AR, Mobley HL. Preventing urinary tract infection: progress toward an effective Escherichia coli vaccine. Expert Rev Vaccines. 2012;11(6):663-76.
31. Poggio TV, La Torre JL, Scodeller EA. Intranasal immunization with a recombinant truncated FimH adhesin adjuvanted with CpG oligodeoxynucleotides protects mice against uropathogenic Escherichia coli challenge. Canadian journal of microbiology. 2006;52(11):1093-102.
32. Palaszynski S, Pinkner J, Leath S, Barren P, Auguste CG, Burlein J, et al. Systemic immunization with conserved pilus-associated adhesins protects against mucosal infections. Developments in biological standardization. 1998;92:117-22.
33. Eldridge GR, Hughey H, Rosenberger L, Martin SM, Shapiro AM, D'Antonio E, et al. Safety and immunogenicity of an adjuvanted Escherichia coli adhesin vaccine in healthy women with and without histories of recurrent urinary tract infections: results from a first-in-human phase 1 study. Hum Vaccin Immunother. 2021;17(5):1262-70.
34. Starks CM, Miller MM, Broglie PM, Cubbison J, Martin SM, Eldridge GR. Optimization and Qualification of an Assay that Demonstrates that a FimH Vaccine Induces Functional Antibody Responses in Women with Histories of Urinary Tract Infections. Human vaccines & immunotherapeutics. 2020:1-10.

35. Sauer FG, Remaut H, Hultgren SJ, Waksman G. Fiber assembly by the chaperone-usher pathway. Biochimica et biophysica acta. 2004;1694(1-3):259-67.
36. Tchesnokova V, Aprikian P, Kisiela D, Gowey S, Korotkova N, Thomas W, et al. Type 1 fimbrial adhesin FimH elicits an immune response that enhances cell adhesion of Escherichia coli. Infect Immun. 2011;79(10):3895-904.
37. Kisiela DI, Rodriguez VB, Tchesnokova V, Avagyan H, Aprikian P, Liu Y, et al. Conformational inactivation induces immunogenicity of the receptor-binding pocket of a bacterial adhesin. Proceedings of the National Academy of Sciences of the United States of America. 2013;110(47):19089-94.
38. McLellan JS, Chen M, Joyce MG, Sastry M, Stewart-Jones GB, Yang Y, et al. Structure-based design of a fusion glycoprotein vaccine for respiratory syncytial virus. Science. 2013;342(6158):592-8.
39. Riley TP, Chou HT, Hu R, Bzymek KP, Correia AR, Partin AC, et al. Enhancing the Prefusion Conformational Stability of SARS-CoV-2 Spike Protein Through Structure-Guided Design. Front Immunol. 2021;12:660198.
40. Nguyen HT, Qualizza A, Anang S, Zhao M, Zou S, Zhou R, et al. Functional and Highly Cross-Linkable HIV-1 Envelope Glycoproteins Enriched in a Pretriggered Conformation. J Virol. 2022;96(8):e0166821.
41. Milder FJ, Jongeneelen M, Ritschel T, Bouchier P, Bisschop IJM, de Man M, et al. Universal stabilization of the influenza hemagglutinin by structure-based redesign of the pH switch regions. Proc Natl Acad Sci U S A. 2022;119(6).
42. Wong S, Jin JP. Antibody Epitope Analysis to Investigate Folded Structure, Allosteric Conformation, and Evolutionary Lineage of Proteins. Protein Pept Lett. 2017;24(11):996-1007.
43. Kleeb S, Pang L, Mayer K, Eris D, Sigl A, Preston RC, et al. FimH antagonists: bioisosteres to improve the in vitro and in vivo PK/PD profile. J Med Chem. 2015;58(5):2221-39.
44. Vetsch M, Sebbel P, Glockshuber R. Chaperone-independent folding of type 1 pilus domains. J Mol Biol. 2002;322(4):827-40.
45. Tchesnokova V, Aprikian P, Yakovenko O, Larock C, Kidd B, Vogel V, et al. Integrin-like allosteric properties of the catch bond-forming FimH adhesin of Escherichia coli. J Biol Chem. 2008;283(12):7823-33.
46. Sauer MM, Jakob RP, Eras J, Baday S, Eriş D, Navarra G, et al. Catch-bond mechanism of the bacterial adhesin FimH. Nature Communications. 2016;7:10738.
47. Ceballos-Alcantarilla E, Merkx M. Understanding and applications of Ser/Gly linkers in protein engineering. Methods in enzymology. 2021;647:1-22.
48. Kisiela DI, Avagyan H, Friend D, Jalan A, Gupta S, Interlandi G, et al. Inhibition and Reversal of Microbial Attachment by an Antibody with Parasteric Activity against the FimH Adhesin of Uropathogenic E. coli. PLOS Pathogens. 2015;11(5):e1004857.
49. Sevier CS, Kaiser CA. Formation and transfer of disulphide bonds in living cells. Nat Rev Mol Cell Biol. 2002;3(11):836-47.
50. Jones CH, Pinkner JS, Nicholes AV, Slonim LN, Abraham SN, Hultgren SJ. FimC is a periplasmic PapD-like chaperone that directs assembly of type 1 pili in bacteria. Proc Natl Acad Sci U S A. 1993;90(18):8397-401.
51. Hull RA, Gill RE, Hsu P, Minshew BH, Falkow S. Construction and expression of recombinant plasmids encoding type 1 or D-mannose-resistant pili from a urinary tract infection Escherichia coli isolate. Infect Immun. 1981;33(3):933-8.
52. Cespedes S, Saitz W, Del Canto F, De la Fuente M, Quera R, Hermoso M, et al. Genetic Diversity and Virulence Determinants of Escherichia coli Strains Isolated from Patients with Crohn's Disease in Spain and Chile. Front Microbiol. 2017;8:639.

53. Bouckaert J, Berglund J, Schembri M, De Genst E, Cools L, Wuhrer M, et al. Receptor binding studies disclose a novel class of high-affinity inhibitors of the Escherichia coli FimH adhesin. Mol Microbiol. 2005;55(2):441-55.
54. Kisiela DI, Rodriguez VB, Tchesnokova V, Avagyan H, Aprikian P, Liu Y, et al. Conformational inactivation induces immunogenicity of the receptor-binding pocket of a bacterial adhesin. Proc Natl Acad Sci U S A. 2013;110(47):19089-94.
55. Sauer MM, Jakob RP, Luber T, Canonica F, Navarra G, Ernst B, et al. Binding of the Bacterial Adhesin FimH to Its Natural, Multivalent High-Mannose Type Glycan Targets. J Am Chem Soc. 2019;141(2):936-44.
56. Kisiela DI, Magala P, Interlandi G, Carlucci LA, Ramos A, Tchesnokova V, et al. Toggle switch residues control allosteric transitions in bacterial adhesins by participating in a concerted repacking of the protein core. PLoS pathogens. 2021;17(4):e1009440-e.
57. Graham BS, Gilman MSA, McLellan JS. Structure-Based Vaccine Antigen Design. Annu Rev Med. 2019;70:91-104.
58. Musunuri S, Weidenbacher PAB, Kim PS. Bringing immunofocusing into focus. NPJ Vaccines. 2024;9(1):11.
59. McCormick JK, Tripp TJ, Olmsted SB, Matsuka YV, Gahr PJ, Ohlendorf DH, et al. Development of streptococcal pyrogenic exotoxin C vaccine toxoids that are protective in the rabbit model of toxic shock syndrome. J Immunol. 2000;165(4):2306-12.
60. Donald RGK, Flint M, Kalyan N, Johnson E, Witko SE, Kotash C, et al. A novel approach to generate a recombinant toxoid vaccine against Clostridium difficile. Microbiology (Reading). 2013;159(Pt 7):1254-66.
61. McLeod B, Mabrouk MT, Miura K, Ravichandran R, Kephart S, Hailemariam S, et al. Vaccination with a structure-based stabilized version of malarial antigen Pfs48/45 elicits ultra-potent transmission-blocking antibody responses. Immunity. 2022;55(9):1680-92 e8.
62. Sokurenko EV, Tchesnokova V, Interlandi G, Klevit R, Thomas WE. Neutralizing Antibodies Against Allosteric Proteins: Insights From a Bacterial Adhesin. J Mol Biol. 2022;434(17):167717.
63. Abernathy ME, Dam KA, Esswein SR, Jette CA, Bjorkman PJ. How Antibodies Recognize Pathogenic Viruses: Structural Correlates of Antibody Neutralization of HIV-1, SARS-CoV-2, and Zika. Viruses. 2021;13(10).
64. Friedrich N, Stiegeler E, Glogl M, Lemmin T, Hansen S, Kadelka C, et al. Distinct conformations of the HIV-1 V3 loop crown are targetable for broad neutralization. Nat Commun. 2021;12(1):6705.
65. Begier E, Rosenthal NA, Gurtman A, Kartashov A, Donald RGK, Lockhart SP. Epidemiology of Invasive Escherichia coli Infection and Antibiotic Resistance Status Among Patients Treated in US Hospitals: 2009-2016. Clinical infectious diseases : an official publication of the Infectious Diseases Society of America. 2021;73(4):565-74.
66. Schembri MA, Hasman H, Klemm P. Expression and purification of the mannose recognition domain of the FimH adhesin. FEMS Microbiol Lett. 2000;188(2):147-51.
67. Emsley P, Cowtan K. Coot: model-building tools for molecular graphics. Acta Crystallogr D Biol Crystallogr. 2004;60(Pt 12 Pt 1):2126-32.